Molecular recognition and imaging of human telomeric G-quadruplex DNA in live cells: A systematic advancement of thiazole orange scaffold to enhance binding specificity and inhibition of gene expression

Wei Long, Bo-Xin Zheng, Xuan-He Huang, Meng-Ting She, Ao-Lu Liu, Kun Zhang*, Wing-Leung Wong* and Yu-Jing Lu*

ABSTRACT

A series of fluorescent ligands, which were systematically constructed from thiazole orange scaffold was investigated for their interactions with G-quadruplex structures and antitumor activity. Among the ligands, compound **3** was identified to exhibit excellent specificity towards telomere G4-DNA over other nucleic acids. The affinity of **3**-Htg24 was almost 5 times higher than that of double-stranded DNA and promoter G4-DNA. Interaction studies showed that **3** may bind to both G-tetrad and the lateral loop near 5'-end. The intracellular co-localization with BG4 and competition studies with BRACO19 reveal that **3** may interact with G4-structures. Moreover, **3** reduces the telomere length and downregulates hTERC and hTERT mRNA expression in HeLa cells. The cytotoxicity of **3** against cancer cells (IC_{50} =12.7–16.2 μM) was found generally higher than non-cancer cells (IC_{50} =52.3 μM). The findings may support that the ligand is telomere G4-DNA specific and may provide meaningful insights for anticancer drug design.

INTRODUCTION

Nucleic acids can form many subtle secondary structures including the non-canonical DNA and RNA G-quadruplexes (G4).[1–4] These special structures may play vital roles in biological process such as regulation of gene expression and cell proliferation.[5–8] The putative G4-forming sequences are prevalently found in the human genome and are localized in the biologically relevant regions such as telomeres,[9–11] which implicate in many critical cellular process underlying genome stability, cancer, and aging.[12–14] The length of telomeres is progressively shortened after each round of DNA replication and cell division and eventually the remaining small segments can no longer be copied, which is referred as "the end replication problem". Nonetheless, Greider and Blackburn discovered that telomerase plays a key role in the addition of TTAGGG repeats to telomeres.[15] Telomerase is found over expressed in many tumor cells and, during the telomerase activity, the telomeric G4-DNA structure needs to be unfolded.[16–18] To enhance the stability of G4-structures with ligands may be able to inhibit the telomerase activity.[19,20] The telomeric G4-DNA structure is thus a potential drug target for chemical biology and anticancer research.

Over the past decade, a variety of ligands selectively binding to telomeric G4-DNAs have been reported. Some typical examples such as telomestatin,[21] TMPyP4,[22] Se2SAP,[23] PDC-360A,[24] Phen-DC3,[25] BRACO19,[26] CND-1,[27] and phthalocyanine[28] for the inhibition of telomerase activity have been demonstrated. To design low molecular mass fluorescent ligands possessing high specificity and affinity targeting telomeric G4-structures for chemical biology study is challenging. Thiazole orange (TO) is a nonspecific ligand and is widely utilized for nucleic acid staining due to its excellence in fluorescence quantum yield.[29] Some recent works such as benzofuroquinolinium,[30] ISTO,[31] TOPI,[32] and PyroTASQ[33] have also demonstrated that the structural modification of TO can offer a notable telomeric G4-DNA specificity in terms of fluorescence discrimination. In addition, several styryl-substituted TO molecules have been reported to show better selectivity towards G4s and ribosomal RNA over other nucleic acid substrates depending on the scaffold of the group substituted at the *ortho*-position of the 1-

methylquinolinium ring.[34,35] However, a systematic engineering of TO on the benzothiazole and 1-methylquinolinium moieties for understanding the binding specificity towards G4-DNA structures is rarely found in literature. We reported herein a series of systematically designed styryl-substituted TO ligands and the study of the structural influence on the specificity and binding affinity towards various G4-structures and their complementary i-motif scaffolds. In addition, the effects of the ligand on the inhibition of telomeric G4-DNA amplification *in vitro*, the inhibition of telomerase activity, the downregulation of hTERC and hTERT expression, the cytotoxicity evaluation against the cancer and non-cancer cells, and the application of the ligand in cell imaging and intracellular localization of G4-structures were demonstrated.

RESULTS AND DISCUSSION

The design of telomeric G4-DNA specific binding molecules and their photophysical properties. To have a better understanding of the structural relationship of the ligands in ligand-DNA interactions targeting G4-structures, a series of fluorescent ligands constructed based on the thiazole orange scaffold with a variety of substituents as shown in Scheme 1 (**1–10**) was rationally designed and synthesized. The ligands isolated for assays were confirmed to have a purity not less than 95% with HPLC analysis and their water solubility at 25 °C was determined to be in the range of 71–167 μM. The specificity of these ligands towards different G4-structures was screened using fluorescence titrations with a panel of representative nucleic acids (Table S1) including single-stranded, double-stranded and G-quadruplexes (promoter and telomere) DNA, i-motif, and rRNA in a buffer solution containing 60 mM KCl at pH 7.4. The induced fluorescence intensity due to ligand-DNA interactions indicates the discrimination ability of the ligand towards a specific G4-structure. The screening results (Figure S1–S2) revealed that the substituent groups of the ligands exhibit significant influence on the binding selectivity with different nucleic acids. In the molecular design, we took two-site modifications on the thiazole orange scaffold (Scheme 1): (i) Substitution at the nitrogen atom of the thiazole ring with two variable groups possessing

similar size (one polar and one less polar), 4-propylmorpholine and 4-methyl-1-propylpiperidine; (ii) Substitution at the 2-position of 1-methylquolinediunium moiety with five variable groups bearing different polarity and size. By analysis of the structures with regard to the discrimination signal induced from the ligand-DNA interaction, we found that the substituent group of *p*-dimethylaminostyryl at the 2-position of the 1-methylquolinediunium site is the most critical to achieve good telomeric G4-DNA discrimination against other type of nucleic acids. Moreover, the combination with a 4-propylmorpholine substituent at the nitrogen atom of the thiazole ring (ligand **3**) offers the best G4-specificity targeting telomere DNA such as Htg24, Htg22 and Telo21 while its analogue **8** bearing a 4-methyl-1-propylpiperidine substituent at same site is less specific because the substrates of double-stranded DNA and promoter G4-DNA were also showed significant interaction signals.

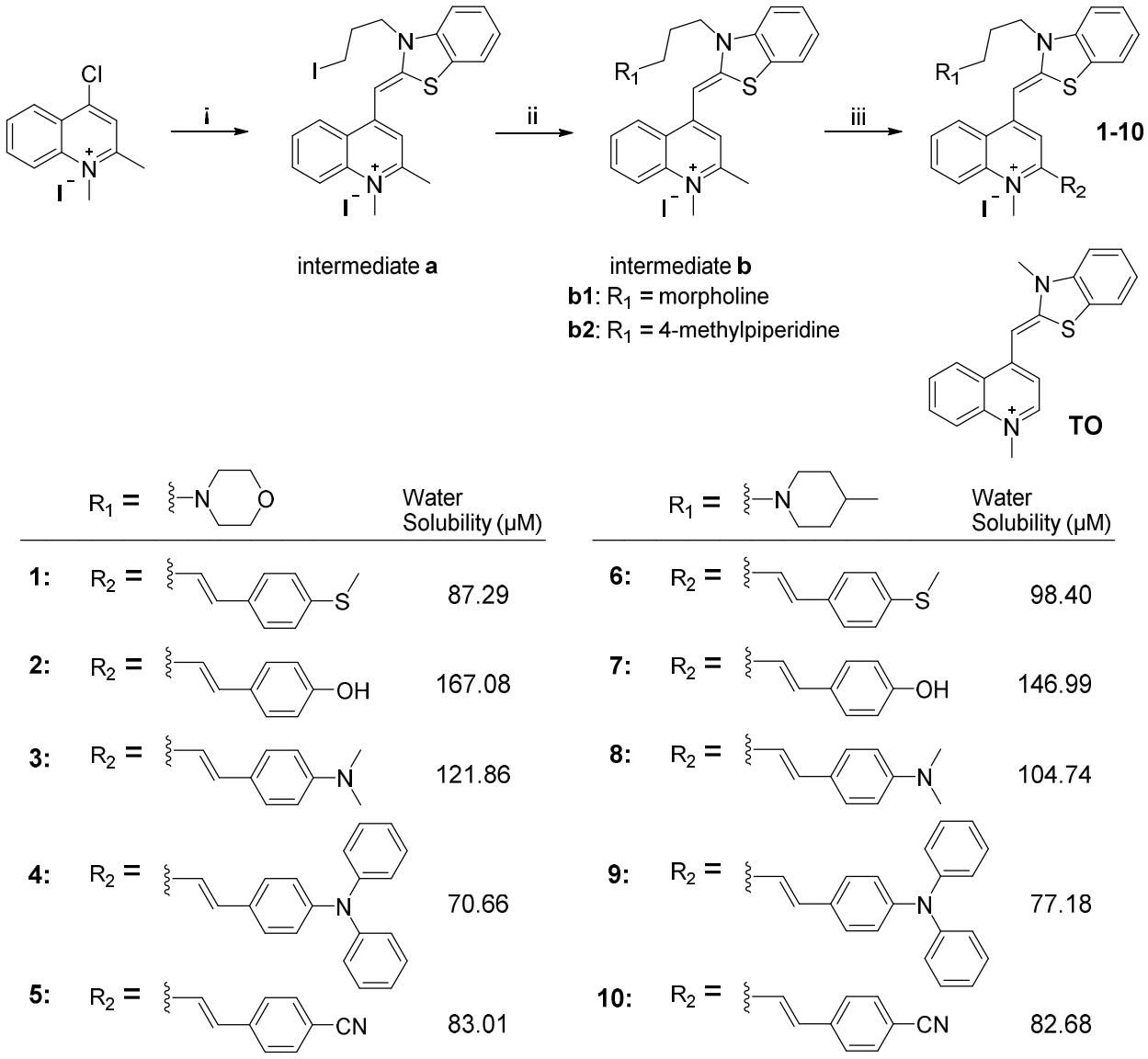

Scheme 1. Synthetic routes to compounds **1–10**. (i) Reaction of 4-chloro-1,2-dimethylquinolin-1-ium iodide, 3-(3-iodopropyl)-2-methylbenzo[*d*]thiazol-3-ium bromide and potassium iodide in methanol solution, at 40 °C for 3 h; recrystallization of crude products with ether to obtain intermediate **a** in 80 % yield. (ii) Reaction of intermediate **a** with morpholine (or 4-methylpiperidine) in acetonitrile, at 40 °C for 24 h; recrystallization of crude products with ether to obtain the intermediate **b1** or **b2** in 40-50% yield. (iii) Reaction of intermediate **b1** (or **b2**) and 4-(methylthio)benzaldehyde (or 4-hydroxybenzaldehyde, or 4-(dimethylamino)benzaldehyde, or 4-(diphenylamino)benzaldehyde, or 4-formylbenzonitrile) with 4-methylpiperidine as a base in n-butyl alcohol, reflux (about 135 °C) for 3 h; purification of crude products by flash silica gel column chromatography to obtain compounds **1-10**.

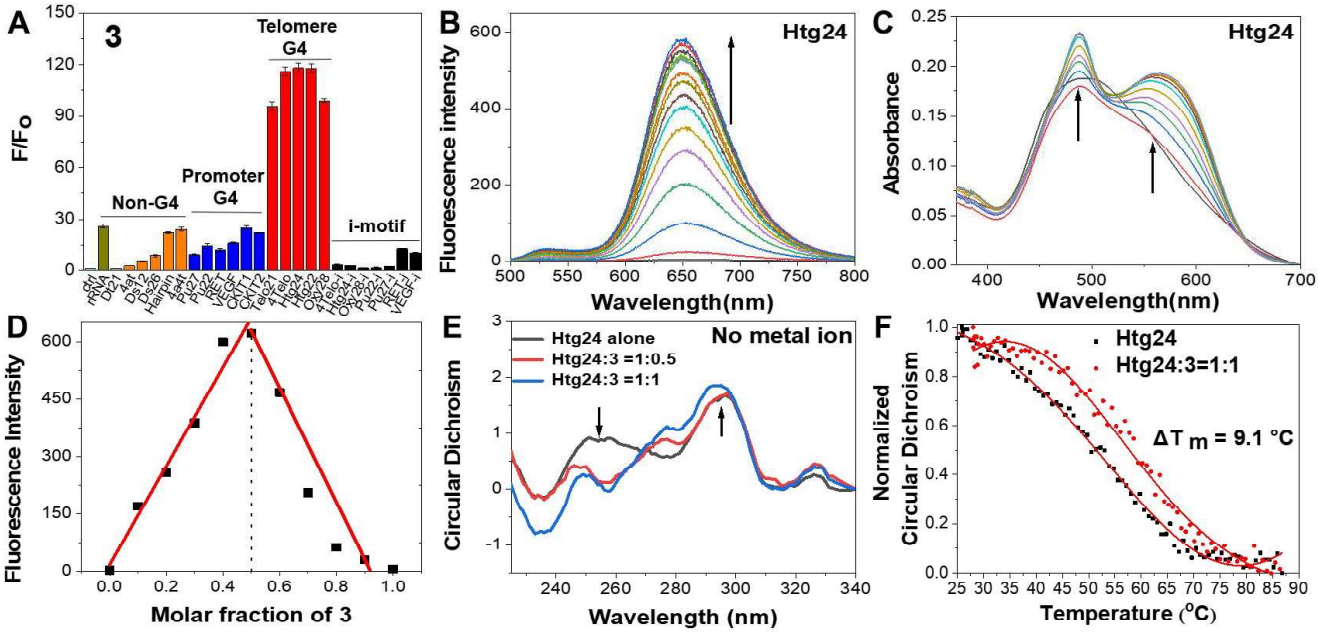

Figure 1. The specificity of ligand **3** to recognize G4-DNA to induce fluorescence signal. (A) Selectivity screening based on induced fluorescent responses of **3** upon bound with various nucleic acids in a pH 7.4 Tris-HCl buffer (10 mM) containing 60 mM KCl. The ligand concentration was 5 μM with DNA substrates at 15 μM. The control is the test solution containing same concentration of ligand and without adding DNA substrates. (B) Fluorescence titration spectra of **3** with Htg24 G4-DNA in a pH 7.4 Tris-HCl buffer (10 mM) containing 60 mM KCl. (C) Ultraviolet Spectrophotometric titrations of **3** (5 μM) with Htg24 (0−15 μM) in a pH 7.4 Tris-HCl buffer (10 mM) containing 60 mM KCl. (D) The Job plot analysis of binding stoichiometry of **3** and Htg24; (E) CD spectra of 5 μM Htg24 binding with **3** at pH 7.4 in a Tris-HCl buffer (10 mM) without metal ion; (F) CD melting curves for Htg24 G4-DNA with or without the addition of **3** (5 μM).

The spectral property of binding ligands is one of the fundamental parameters to be considered for applications in biosensing and bioanalytical purposes, particularly the fluorescence quantum yields. The spectral properties of the ligands **(1–10)** in a buffer solution containing nucleic acids were thus measured (Table S3). The fluorescence quantum yields (Φ_f) of the ligands upon bound to Htg24 were found in the range of 0.045 to 0.317. Moreover, among the ligands, **3** and **8** show long wavelength emission at 642–648 nm (λ_{ex} at 480–483 nm), large Stokes shift (162–165 nm) and good quantum yield (Φ_f = 0.217 and 0.317). Interestingly, **3** demonstrated the best G4-DNA specificity from the screening results. We therefore used this ligand for an in-depth study to understand its interaction mechanism with telomeric G4-DNA *in vitro* and to investigate the recognition property and imaging ability targeting G4-structures in live cells. The control experiment showed that **3** has almost no background fluorescence signal in buffer solution (Figure 1A). When it interacted with telomeric G4-DNA (Htg24 and Htg22), a signal enhancement of 120-fold (F/F_0) was induced, which is about 4–6 times of the promoter G4-DNA, 5–20 times of double-stranded DNA and 50 times of single-stranded DNA. In addition, the interaction of **3** with the i-motif structures examined induced only weak fluorescence signal (F/F_0 = 1–14 folds), which is much lower than that of the G4-structures of their complementary sequences. The results indicate that the ligand may preferentially interact with G4-DNA structures more than their complementary i-motif.[36] In addition, both the fluorescence and UV-vis titrations (Figure 1B–C) indicate the *in-situ* formation of **3**-Htg24 complex. The ligand also shows a good linear relationship between the fluorescence signal induced and the concentration of substrates. The detection limit (LOD) estimated for Htg24 was found to be 86.2 nM approximately (Table S3 and Figure S3). Furthermore, **3** can be utilized as a sensitive and selective fluorescent staining agent for PAGE staining of telomeric G4-DNA substrates such as Telo21, Htg24, Oxy28 because the promoter G4-DNA (such as Pu27 and CKIT2) and dsDNA (Ds26) gave very weak staining signals (Figure S4).

Table 1. Equilibrium binding constants for ligands interacted with various nucleic acids at 25 °C.[a]

Ligand	Equilibrium binding constant, K_{eq} ($\times 10^5$ M^{-1})					
	Dt21	Ds26	rRNA	Pu22	Telo21	Htg24
1	n.d.	6.57±0.12	7.64±0.15	4.86±0.32	3.01±0.09	3.25±0.25
2	n.d.	n.d.	n.d.	12.00±0.25	9.65±0.11	11.99±0.34
3	n.d.	3.67±0.15	6.20±0.11	3.09±0.09	18.52±0.10	20.82±0.22
4	n.d.	2.72±0.03	n.d.	6.45±0.10	5.23±0.16	4.90±0.15
5	n.d.	3.79±0.08	5.01±0.06	4.43±0.05	7.22±0.06	5.05±0.09
6	n.d.	7.55±0.15	7.87±0.26	7.66±0.20	6.50±0.14	6.89±0.12
7	n.d.	14.00±0.52	14.63±0.35	5.50±0.19	13.63±0.25	13.15±0.24
8	n.d.	10.76±0.41	8.40±0.33	16.63±0.41	24.40±0.43	23.52±0.70
9	n.d.	1.54±0.02	n.d.	9.07±0.10	7.85±0.10	7.22±0.05
10	n.d.	13.21±0.15	7.86±0.08	9.83±0.05	9.57±0.03	9.02±0.06

[a] Equilibrium binding constant between the compound and nucleic acid at 25 °C;

n.d.: denotes not determined due to the ligand-DNA binding signal is too weak for estimation.

The binding stoichiometry of the ligand-G4-DNA complex determined by Job plot analysis was found to be 1:1 (Figure 1D). The possible conformational influence of the ligand on Htg24 was studied with circular dichroism (CD) experiments. It is noteworthy that **3** promoted G4-DNA formation under Na^+ or K^+ ion free conditions (Figure 1E and Figure S5). Moreover, **3** is able to stabilize Htg24 G4-structure in a buffered solution containing KCl (60 mM) at pH 7.4 by increasing 9.1 °C approximately (Figure 1F), indicating the formation of a stable **3**-Htg24 complex. The binding affinity for the ligands showing strong interaction signal with substrates in the fluorescence titrations was estimated (Table 1). By comparing their equilibrium binding constants (K_{eq}), the interaction specificity of the ligand could be more indicative. The results revealed that **3** exhibited the best specificity towards the telomeric G4-DNAs against

promoter G4-DNA (Pu22, K_{eq} =3.1x10^5 M^{-1}), single-stranded (Dt21, the interaction was too weak for determination) and double-stranded DNA (Ds26, K_{eq} =3.7x10^5 M^{-1}), and rRNA (K_{eq} =6.2x10^5 M^{-1}). The affinity of **3** interacted with Htg24 was found to be about 20.8x10^5 M^{-1}, which is at least 3-fold higher than other type of nucleic acids. The binding constants estimated from fluorescence titrations were found comparable with those obtained from isothermal titration calorimetry (Table S4 and Figure S6–S8). The interaction affinity in terms of K_d values for **3**-Htg24 (K_d =0.65 μM) and **3**-Htg22 (K_d =0.71 μM) is at least 4-fold stronger than that of **3**-Pu27 (K_d =3.27 μM) and **3**-Ds26 (K_d =2.97 μM). We therefore speculated that the molecular scaffold of **3** may have a better site-matching with the binding pocket of the telomeric G4-structure, such as Htg24, which rendered it a good discrimination against those of promoter G4-DNA structures such as Pu22 and Pu27. Further supportive results were obtained from the study of ligand–G4-DNA interactions in solution with ^{1}H NMR titrations and site mutation experiments.

NMR study of ligand-telomeric G4−DNA interaction and probing the binding mode in solution. The ^{1}H NMR study for the interaction of Htg24 with **3** in solution was showed in Figure 2A. The imino protons of Htg24 give a group of characteristic guanine imine proton signals with chemical shifts between 10.5–12.3 ppm, which indicates the formation of G-tetrads.[37,38] In the titration, as increasing the molar ratio of ligand to Htg24, **3** interacts with the guanine bases of the G-tetrad and therefore causes observable changes both in chemical shift and peak intensity of the imino proton signals. It was obvious to observe that 8 groups of the imino proton peaks corresponding to the guanine bases G3, G17, G21, G5, G15, G23, G16 and G22 were influenced notably under the titration condition of **3**:Htg24 = 3:1. The peak intensity of G3, G21, G5, G15, and G22 was found decreased. The chemical shift of the peaks corresponding to G16 and G21 was shifted to low field while those of G5 and G23 were shifted to high field. The remaining imino proton signals did not show observable changes. These results suggest that **3** may interact with the G-tetrad through an end-stacking mode. To understand further whether the ligand interacts with these

sites and also with the lateral loop of the telomeric G4-structure, a series of single-site mutations on an Htg24 sequence was investigated (Figure S9). The topology of Htg24 wild type is antiparallel in buffer solution with 60 mM K^+ ion and no conformational change was observed upon interacted with **3** (Figure S5). Nonetheless, circular dichroism (CD) measurements for Htg24 mutants revealed conformational changes for certain mutation sites including T6G (hybrid), A8G (hybrid), T12G (hybrid), A14G (hybrid), G16A/C/T (parallel), T18G (hybrid), T19G (hybrid), A20G (hybrid) and G22A/C/T (hybrid) while the remaining mutants retained the antiparallel conformation. It is noteworthy that the interaction of ligand with all these mutants does not induce conformational changes (Figure S10).

In addition, Figure 2B showed that the remarkable negative impacts in fluorescence titrations for the interaction signal were found on the mutants at the sites of G3A/C/T, G5C, T6G, A14G, G16A/C/T, G17A/C/T, T18G, A20G and G22A/C/T, while the mutants at sites G21A/C/T showed very strong signal enhancement unexpectedly. It is noteworthy that the influence of interaction signal at mutation sites of G23, G15 and G11 was found relatively mild. From an Htg24 model shown in Figure 2B, G3, G17 and G21 are the core guanine bases of the terminal G-tetrad near 5'-end. T6, T18 and A20 are on the lateral loops, which are also located near 5'-end. Moreover, it is interesting to observe that the mutations of G21A/C/T, as altering its location from G-tetrad to the lateral loop, the interaction signal was intensified but caused no conformational changes. All these results may indicate that the interaction mode of **3**-Hgt24 could probably involve the lateral loop binding. Furthermore, the remarkable influence on the interaction signals observed at these particular sites may suggest that the interaction of **3**-Hgt24 most likely occurs at the binding pocket near 5'-end through an end-stacking mode with the G-tetrad and its side groups may interact with the adjacent lateral loops. Taken together, the results obtained from mutations study are found consistent with the NMR observation. It may also support that the ligand probably has a preferential interaction mode of end-stacking with G-tetrad in combination with the lateral loop interaction near 5'-end.

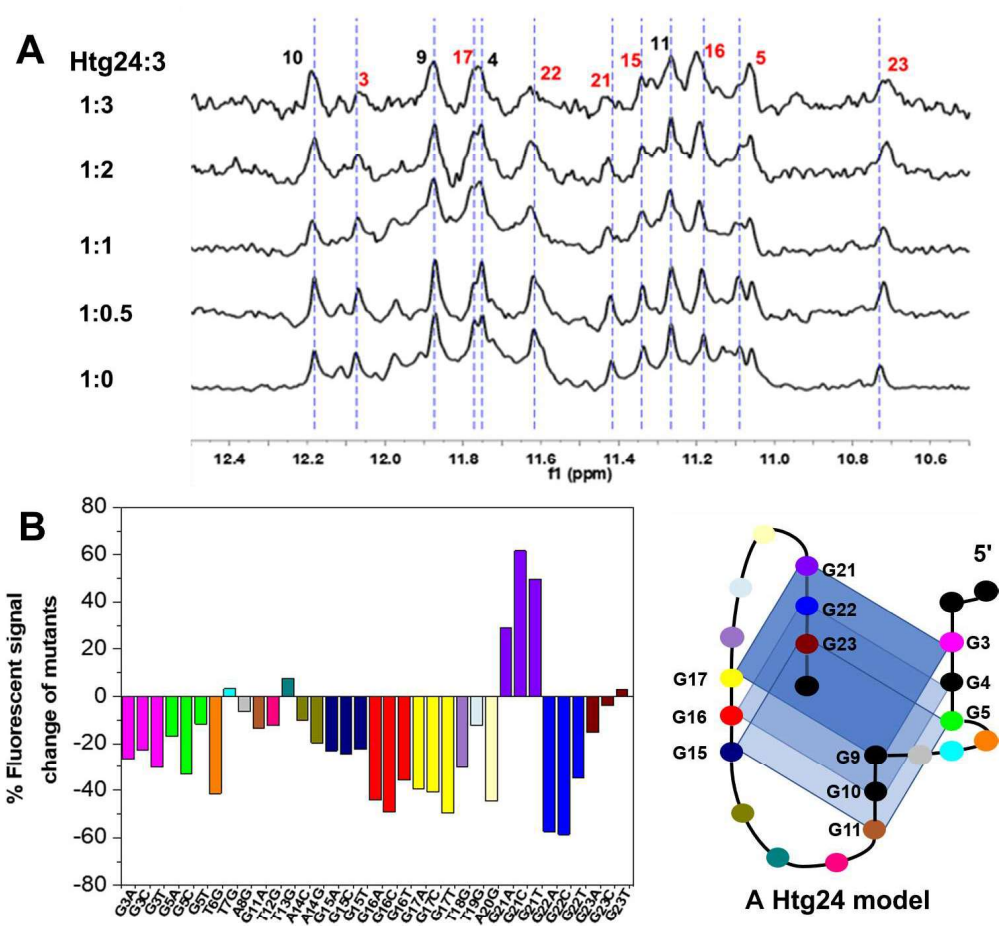

Figure 2. (A) The ^{1}H NMR spectra showed the imino proton regions of Htg24 and its interaction with **3** at a molar ratio from 1:0.5 to 1:3. The titrations were performed in a 25 mM KH_2PO_4 buffer (10% D_2O, 70 mM KCl, pH 7.4) at 25 °C. (B) Fluorescence binding assays of **3** (5 μM) with Htg24 mutants in a Tris–HCl buffer containing 60 mM KCl. The fluorescence signal change = ($F_{Htg24\ mutant}$ - $F_{Htg24\ wild\ type}$)/$F_{Htg24\ wild\ type}$.

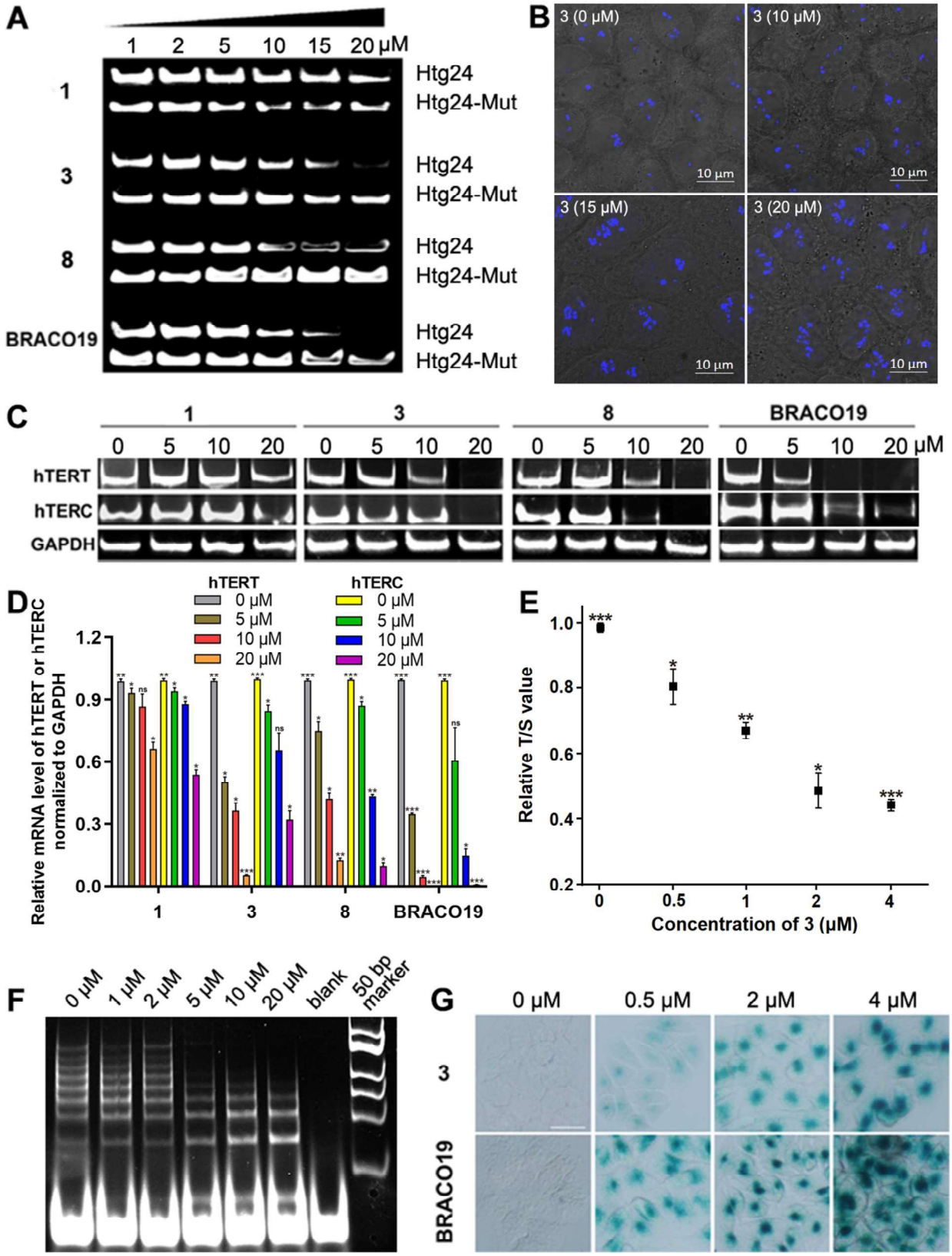

Figure 3. (A) The stabilization ability of ligands (**1**, **3**, **8** and BRACO19) on Htg24 G4-DNA was detected by PCR stop method. The mutation sequence was designed specifically to prevent the formation of G4-

DNA. All strips were dyed by SYBR Gold. (B) An increasing observable BG4 foci in HeLa cells after treated with **3** (0–20 μM). (C) qRT-PCR products were separated by electrophoresis in a 3% agarose gel and were stained with SYBR Gold. (D) The mRNA expression of hTERC and hTERT genes detected by real-time qRT-PCR. All the data represented the relative fold change of mRNA expression of the hTERT and hTERC genes. (ns: $p>0.05$, *$p<0.05$, **$p<0.01$, ***$p<0.001$). (E) Relative telomere length measurement results: HeLa cells were treated with **3** at 0–4 μM for 18 days. (ns: $p>0.05$, *$p<0.05$, **$p<0.01$, ***$p<0.001$). (F) Concentration-dependent inhibition of telomerase activity by **3** in HeLa cells. (G) SA-*β*-gal assays were used to investigate the effects of **3** and BRACO19 on cell senescence of HeLa cells.

Stabilization of telomere G4-DNA structure *in vitro* and in cells with the ligand. Since compound **3** is able to bind to telomeric G4-DNA selectively and stabilizes the G4-structure, we further examined its ability to inhibit the amplification of the telomere G4-forming sequence *in vitro*. Figure 3A showed the results of PCR stop assays, in which a G4-forming DNA oligonucleotide Htg24 was treated with **1** (non-G4 selective and weak affinity), **3** (G4-selective with strong affinity) and **8** (less G4-selective and strong affinity), respectively. The mutant (Htg24-Mut) with a non-G4 forming Htg24 sequence was also conducted as a control. In the experiments, applying the ligand at 20 μM, **1** did not inhibit the PCR product formation and **8** showed partially inhibited while **3** completely inhibited the DNA amplification of Htg24 by Taq polymerase. The performance of **3** was found comparable with BRACO19. These results indicate that **3** may interact telomeric G4-DNA and stabilize the G4-structure and thus inhibiting DNA amplification. In addition, in the assays to stain the intracellular G4-structure in HeLa cells with BG4 (Figure 3B), it is noteworthy that the number of observable BG4 foci (blue spots) found in the imaging was increased gradually when the concentration of **3** was increased from 0 to 20 μM for incubation with

HeLa cells. The results demonstrate that **3** may induce the formation of G4-structure and then stabilize the structures in cellular.

Downregulation of the gene expression of hTERC and hTERT *in vivo* and the inhibition of telomerase activity with the ligand. The telomerase is a large complex that consists of many components; however, hTERT and hTERC are the minimal complex required for telomerase activity *in vitro*.[39] In various types of human cancers, the level of hTERT and hTERC gene expression is usually upregulated.[40,41] Nevertheless, the molecular mechanism involved in the regulation of hTERT and hTERC gene expression for telomere maintenance and telomerase activity has not been clear currently.[42] It is noteworthy that the telomerase activity was found not detectable in the absence of hTERC,[43] which may suggest that the downregulation of hTERC expression with ligands in cancer cells could inhibit telomerase activity. To investigate whether the G4-DNA binding ligands could downregulate the hTERC expression, we quantified the total mRNA of hTERC and hTERT in HeLa cells treated with different concentrations of compounds and also compared the results with BRACO19. The results were shown in Figure 3C–D and Figure S11. It was found that both **3** and **8** demonstrated comparable downregulation effects to BRACO19 in the expression of hTERC and hTERT mRNA despite the underlying molecular mechanism remains unclear. In addition, the qRT-PCR results showed that both compounds at 20 μM almost completely inhibited the expression of hTERC and hTERT mRNA, while **1** was found obviously less effective. The downregulation of hTERC and hTERT genes expression *in vivo* may be attributed to the influence of the G4-selective ligands binding to the c-MYC promoter, which is a key regulator to control the transcription of these genes in tumorigenesis.[44,45] The compounds that could proficiently downregulate hTERC and hTERT gene expression and, at the same time, interfere with telomere integrity may be able to achieve high efficacy on the anti-telomerase therapy.[46]

The effect of **3** on the reduction of telomere length and telomerase activity inhibition was also examined. HeLa cells were treated with the ligand for 18 days and then the relative telomere length was measured

with the qRT-PCR based method (Figure S12).[47] The results shown in Figure 3E revealed that **3** reduced notably the telomere length in a concentration-dependent manner, which is probably attributed to the stabilization of telomeric G4-DNA structure with the ligand that interrupts the telomerase activity in HeLa cells. TRAP assays were also conducted to determine the telomerase activity in HeLa cells. From Figure 3F, the results show that **3** is able to inhibit telomerase activity in HeLa cells in a concentration-dependent manner. However, the effect from the downregulation of hTERC and hTERT expression with the G4-binding ligands could also be a possible factor in the inhibition of telomerase activity.[43] Furthermore, **3** and BRACO19 were applied in SA-*β*-gal assays to study and compare their effects on cancer cell senescence (Figure 3G). It is noteworthy that both compounds were positive in SA-*β*-gal staining and showed comparable results, which may infer that **3** interacts with telomere G4-DNA and stabilizes the structures. Consequently, it may cause telomere shortening and/or telomere dysfunction and followed leading to cancer cell senescence. The findings may be in alignment with a previous study that revealed the interaction of BRACO19 with telomere G4-DNA causing viability loss in brain tumor cells due to the ligand inducing T-loop disassembly and telomerase displacement.[48]

Live cell imaging study with the ligand. Live cell imaging performance of **3** targeting telomeric G4-DNA were demonstrated in U87 cells. A commercial dye (DAPI) was applied for comparison. From Figure 4A, the cells after co-staining with DAPI and **3**, the whole nucleus region of the cell was imaged blue by DAPI (λ_{ex}=402 nm) while **3** (green channel λ_{ex}=488 nm or red channel λ_{ex}=571nm) only selectively stained certain areas inside the nucleus with a few spots. These sub-nuclear structures stained are possibly nucleoli. The imaged intranuclear dots suggest that these regions may contain G4 structures. To confirm DNA was stained by the compound, the RNase and DNase digestion assays were conducted. From Figure 4B–C, the cells stained with **3** remained unchanged after treated with RNase. In contrast, after DNase treatment, the fluorescence signals were completely disappeared. The results indicate that the cellular substrate stained is DNA. To further validate the G4-DNA was stained in live cells, co-

localization experiments with a G4-specific antibody (BG4) were conducted. From the confocal images (Figure 4D), BG4 showed some blue foci in the nucleus and **3** also displayed green/red spots in the nucleus and exhibited strong fluorescence intensity in the sub-nuclear structures. The merged images highlight the co-localization area, which support that BG4 and **3** may have the same binding target in cells.

In addition, we used a strong telomeric G4-DNA binding ligand, BRACO19, to compete with **3** in live U87 cells. As shown from Figure 5A–E, the cells stained with **3** showed some bright spots in the nucleus. When the cells were treated with BRACO19 in an increasing concentration manner (0–20 μM), the fluorescence intensity of the stains of **3** were decreased gradually. With 20 μM BRACO19, the stains were completely disappeared. The intracellular competition results obtained in live U87 cells were also found consistent with the *in vitro* competitive experiments shown in Figure 5F, in which **3** bound to Htg24 was gradually displaced by BRACO19 and caused a significant reduction of fluorescence intensity. Taken together, the results indicate that **3** and BRACO19 may have the same binding target both *in vitro* and in live cancer cells.

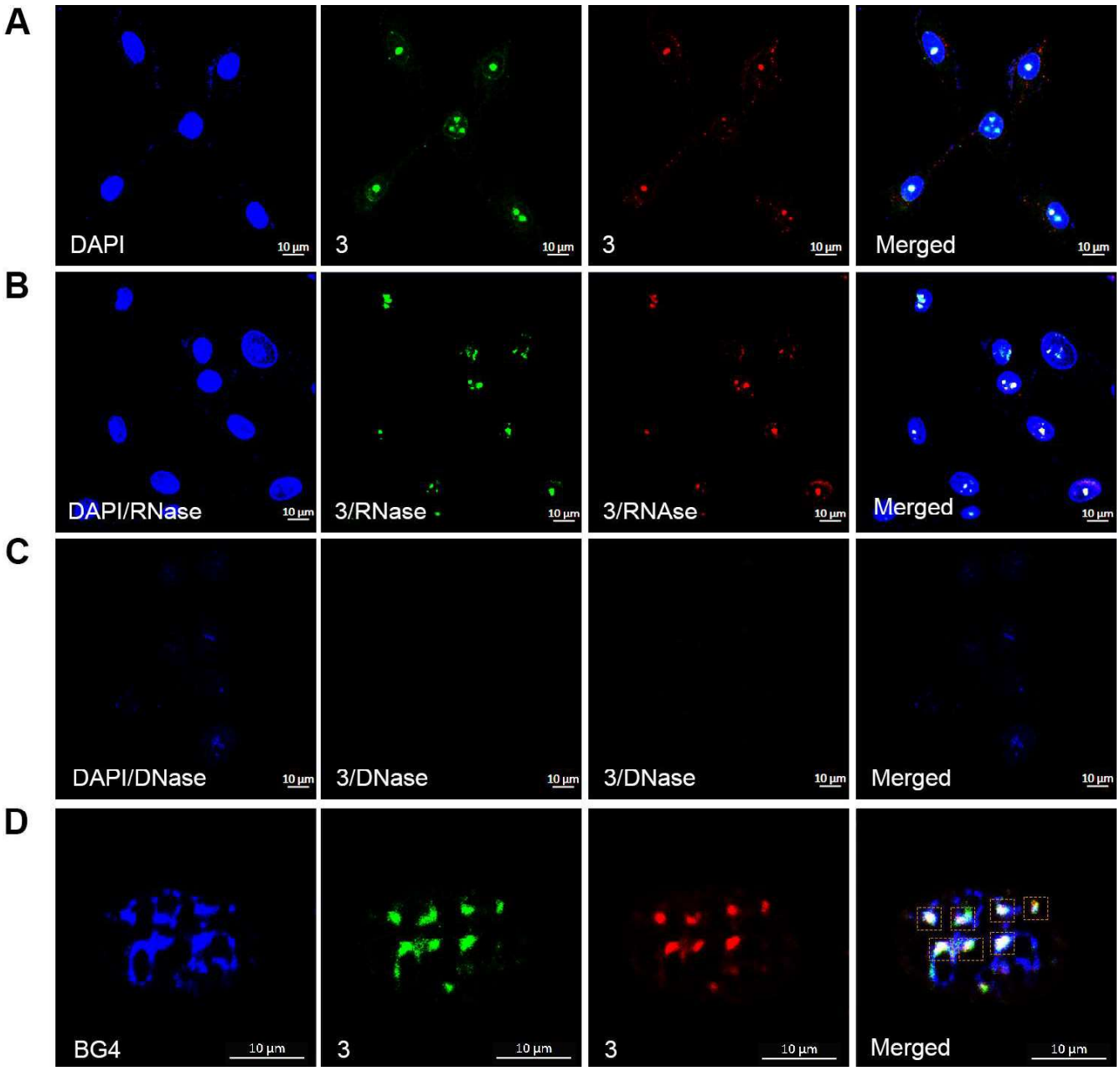

Figure 4. (A) Fluorescence images of live U87 cells co-stained with **3** (5 μM) for 30 min and DAPI (1.0 μM) for 10 min; (B) Fluorescence images of live U87 cells co-stained with **3** (5 μM) for 30 min and DAPI (1 μM) for 10 min and followed with RNase treatment for 30 min; (C) Fluorescence images of live U87 cells co-stained with **3** (5 μM) for 30 min and DAPI (1 μM) for 10 min and followed with DNase treatment for 30 min; (D) Confocal images of U87 cells stained with **3** and BG4 in the immunofluorescence experiments.

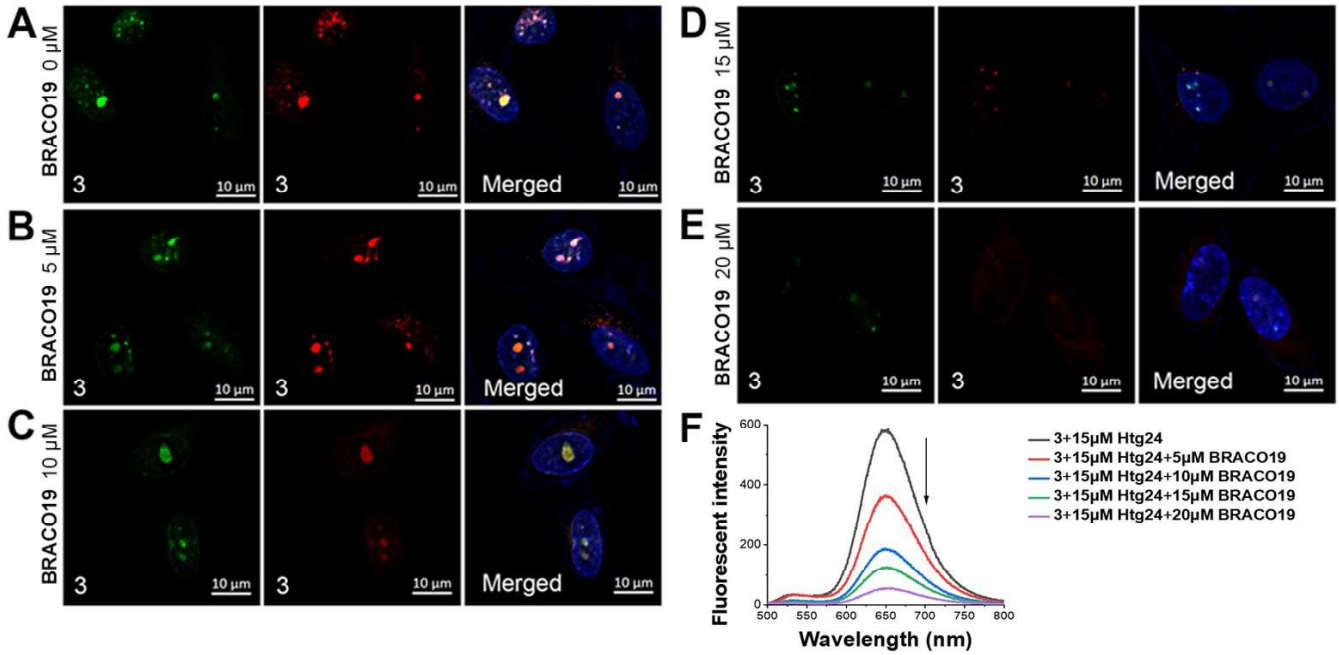

Figure 5. (A) U87 cells stained with **3** (5 μM) and DAPI. (B) U87 cells stained with **3** (5 μM), BRACO19 (5 μM) and DAPI. (C) U87 cells stained with **3** (5 μM), BRACO19 (10 μM) and DAPI. (D) U87 cells stained with **3** (5 μM), BRACO19 (15 μM) and DAPI. (E) U87 cells stained with **3** (5 μM), BRACO19 (20 μM) and DAPI. The cells after staining were imaged with a LSM 800 laser scanning confocal microscope (excitation wavelength was 488 nm or 571 nm for **3** and was 402 nm for DAPI). (F) The competition study of fluorescent signal responses of **3** (5 μM) binding with nucleic acid and increasing BRACO19 (5–20 μM).

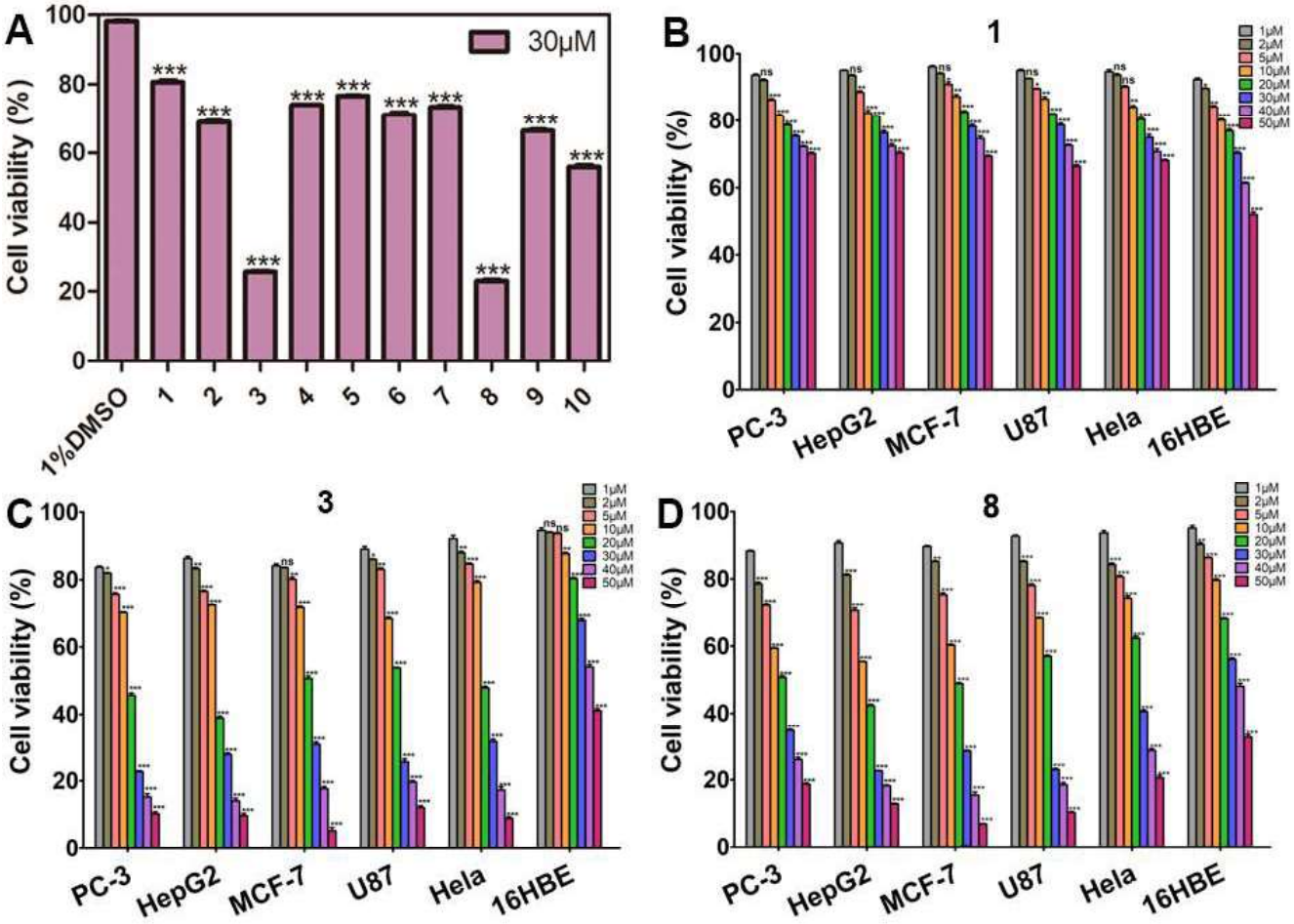

Figure 6. (A) Viability of U87 cells treated with 30 μM of ligands **1–10**; (B) PC3, HepG2, MCF7, U87, HeLa and 16HBE cells treated with **1** (1–50 μM) for 36 h, respectively. (C) PC3, HepG2, MCF7, U87, HeLa and 16HBE cells treated with **3** (1–50 μM) for 36 h, respectively. (D) PC3, HepG2, MCF7, U87, HeLa and 16HBE cells treated with **8** (1–50 μM) for 36 h, respectively. (ns: $p>0.05$, *$p<0.05$, **$p<0.01$, ***$p<0.001$).

Table 2. **IC_{50} (μM) estimated for the compound against various cancer cells and nonmalignant cells.**

Compound	PC3	HepG2	MCF7	U87	HeLa	16HBE
1	91.06±0.66	96.49±0.37	105.3±0.56	96.80±0.52	90.26±0.74	58.02±0.45
3	12.75±0.24	12.82±0.43	14.52±0.31	15.24±0.22	16.26±0.38	52.29±0.48
8	14.56±0.33	11.02±0.26	12.63±0.59	14.69±0.16	21.16±0.56	34.77±0.59

Cytotoxicity of ligands against cancer cells and nonmalignant cells. The development of telomeric G4-specific binding molecules is recognized as an attractive strategy for anticancer therapies because these ligands may potentially trigger telomere dysfunction via the interference with telomerase and telomere maintenance of cancer cells,[49] particularly in telomerase-positive cancer cells. To study whether the new telomeric G4-DNA specific compound showing a broad-spectrum of anticancer activity, we selected a number of cancer cell lines (PC3, HepG2, MCF7, U87 and HeLa) and a nonmalignant cell line (16HBE) for cytotoxicity evaluation by MTT assays. The results were shown in Figure 6A–F and the IC_{50} values were summarized Table 2 for comparison. Compounds **3** and **8** exhibit obvious cytotoxicity *in vitro* and a broad-spectrum anti-tumor activity, while **1** shows almost no cytotoxicity effect on the cancer cells examined (IC_{50} = 90.26–105.3 μM) and is more cytotoxic on the nonmalignant cells (IC_{50} = 58.02 μM). Interestingly, **3** shows cytotoxicity in different degrees against cancer cells and nonmalignant cells. It was found to be more effective in the inhibition of cancer cell proliferation (IC_{50} = 12.75–16.26 μM) than nonmalignant cells (IC_{50} = 52.29 μM, which is about 3 ‑ 4 folds higher than that of cancer cells). However, compound **8** has no such cytotoxic selectivity observed; it shows high cytotoxicity against the cancer cells (IC_{50} = 11.02–21.16 μM) but also has a significant toxicity effect against the nonmalignant cells (IC_{50} = 34.77 μM). Therefore, compound **3**, as compared with **8**, is a better drug candidate for anticancer development. The differential cytotoxicity observed with **3** may be probably due to its excellent binding specificity towards telomere G4-DNA over other type of nucleic acids.

CONCLUSION

In conclusion, a series of styryl-substituted thiazole orange ligands was synthesized and one of the analogues was found to be highly specific towards telomeric G4-DNA structures. The ligand–G4-DNA interaction investigated with ^{1}H NMR titration and single-site mutation using Htg24 as a model showed that the ligand possibly interacted with both G-tetrad and the lateral loop near 5'-end. This interaction mode may be a critical factor that renders a high discrimination ability of the ligand targeting telomeric G4-DNA structures over other types of nucleic acids including promoter G4 and i-motif. The intracellular co-localization with BG4 and the competition study with BRACO19 indicated that the ligand may have the same binding target of G4-DNA in cellular. In addition, qRT-PCR results showed that **3** are able to downregulate the expression of hTERC and hTERT mRNA and that probably also causes inhibitory effects on the telomerase activity. In the evaluation of anticancer activity with the compounds, **3** exhibits much higher cytotoxicity against a number of cancer cells (PC3, HepG2, MCF7, U87, HeLa cells; IC_{50} = 12.8–16.3 μM) than the nonmalignant cells (IC_{50} = 52.3 μM). The SA-*β*-gal assays also support that **3** (at 2–4 μM) is able to proficiently induce senescence in HeLa cells. Taken together, the present study demonstrated systematically the molecular design on the basis of a classical and non-specific thiazole orange scaffold to construct telomeric G4-DNA specific fluorescent binding ligands. The findings may provide significant insight into the molecular design of potent and specific anticancer drugs targeting G4-structures at telomeres.

EXPERIMENTAL SECTION

General procedures for the synthesis of target compounds (1–10). High resolution mass spectra (HRMS) were obtained by Agilent 1260-6230TOF or MALDI-TOF (Ultraflextreme). Using TMS as a reference, ^{1}H and ^{13}C NMR spectra were recorded at 400 MHz and 100 MHz in DMSO-d_6 with a Bruker BioSpin GmbH spectrometer. The high performance liquid chromatography (HPLC) analysis for examining the purity of the compounds was performed on an SHIMADZU LC-16 system using a

Diamonsil C18 column (250 × 4.6 mm, 5 μm) at room temperature with an elution using the mobile phase (MeOH/H_2O = 50:50 v/v). All compounds synthesized for assays were confirmed to have a purity ⩾ 95%. Unless otherwise stated, all chemicals were purchased from commercial and the solvents used were analytical reagent grade and were used without further purification. The oligonucleotides used were synthesized and purified by Shanghai Sangon Biotechnology Co., Ltd. (Shanghai, China). The sequences were listed in (Table S1 and Table S2).

A synthetic route to the compounds **1–10** was shown in supporting information. Compound **a** was obtained by the reaction using a 3-(3-iodopropyl)-2-methylbenzo[d]thiazol-3-ium iodide, 0.889 g, 2.0 mmol) and 4-chloro-1,2-dimethylquinolin-1-ium iodide (0.636 g, 2.0 mmol), potassium iodide (0.332 g, 2.0 mmol) in 40 °C for 24 h. Recrystallization of the crude product with ether to obtain **a** in 80% yield. Further reaction of compound **a** (1.198 g, 2.0 mmol) with morpholine (0.435 g, 10.0 mmol) or 4-methylpiperidine (0.495 g, 10.0 mmol) in 40 °C refluxed for 24 h to afford target compounds, **b1** or **b2**. Recrystallization of the crude product with ether to afford 40-50% yield. Compounds **1–5** were obtained by the reaction of **b1** (0.559 g, 1.0 mmol) and 4-(methylthio)benzaldehyde (0.304 g, 2.0 mmol), 4-hydroxybenzaldehyde (0.244 g, 2.0 mmol), 4-(dimethylamino)benzaldehyde (0.298 g, 2.0 mmol), 4-(diphenylamino)benzaldehyde (0.546 g, 2.0 mmol) or 4-formylbenzonitrile (0.262 g, 2.0 mmol) and 4-methylpiperidine (200 μl), n-butanol (10 mL) in 135 °C refluxed for 3 h. Target compounds **6–10** were obtained by the reaction of **b2** (0.571 g, 1.0 mmol) and 4-(methylthio)benzaldehyde (0.304 g, 2.0 mmol), 4-hydroxybenzaldehyde (0.244 g, 2.0 mmol), 4-(dimethylamino)benzaldehyde (0.298 g, 2.0 mmol), 4-(diphenylamino)benzaldehyde (0.546 g, 2.0 mmol) or 4-formylbenzonitrile (0.262 g, 2.0 mmol) and 4-methylpiperidine (200 μl), n-butanol (10 mL) in 135 °C refluxed for 3 h. The crude products were purified by flash silica gel column chromatography. The pure compounds obtained were confirmed with ^{1}H NMR, ^{13}C NMR and HRMS. The purity of the compounds was confirmed to be ⩾ 95% with HPLC analysis (Figure S14–S23).

Compound **(1)**: *1-methyl-2-((E)-4-(methylthio)styryl)-4-((Z)-(3-(3-morpholinopropyl)benzo[d]thiazol-2(3H)-ylidene)methyl)quinolin-1-ium iodide* was obtained as a brown solid with 66% yield. ^{1}H NMR (400 MHz, DMSO-d_6) δ 8.74 – 8.62 (m, 1H), 8.20 – 8.14 (m, 1H), 8.08 – 8.04 (m, 1H), 8.01 – 7.96 (m, 1H), 7.91 – 7.85 (m, 2H), 7.84 – 7.80 (m, 1H), 7.79 – 7.75 (m, 2H), 7.66 – 7.64 (m, 1H), 7.39 (s, 3H), 6.96 – 6.90 (m, 1H), 4.72 – 4.59 (m, 2H), 4.15 (s, 3H), 3.48 (s, 3H), 2.51 (s, 5H), 2.43 – 2.36 (m, 2H), 2.25 (s, 4H), 1.99 (s, 3H). ^{13}C NMR (100 MHz, DMSO-d_6) δ 188.29, 159.27, 152.28, 148.03, 142.06, 140.75, 139.45, 133.66, 132.04, 129.43, 128.41, 126.94, 126.03, 125.50, 124.62, 124.29, 123.47, 120.84, 119.00, 113.24, 108.33, 87.89, 66.45, 55.28, 53.72, 45.13, 44.04, 38.58, 23.69, 14.80. HRMS m/z: calcd for $C_{34}H_{36}N_3OS_2^+$ [M-I]$^+$ 566.22943; found 566.22958 [M-I]$^+$. HPLC analysis: retention time at 2.814 min eluted with MeOH/H_2O = 50:50 v/v, purity = 95%.

Compound **(2)**: *2-((E)-4-hydroxystyryl)-1-methyl-4-((Z)-(3-(3-morpholinopropyl)benzo[d]thiazol-2(3H)-ylidene)methyl)quinolin-1-ium iodide* was synthesized according to the procedures reported previously.[50] The compound was obtained as a dark brown solid with 65% yield. ^{1}H NMR (400 MHz, DMSO-d_6) δ 9.66 (s, 1H), 8.59 (d, J = 8.1 Hz, 1H), 8.10 (d, J = 8.7 Hz, 1H), 8.01 (d, J = 7.8 Hz, 1H), 7.94 (t, J = 7.9 Hz, 1H), 7.75 (d, J = 8.6 Hz, 2H), 7.68 (d, J = 9.0 Hz, 2H), 7.64 (d, J = 8.7 Hz, 1H), 7.56 (m, 2H), 7.42 (m, 1H), 7.34 (t, J = 7.6 Hz, 1H), 6.85 (d, J = 8.6 Hz, 1H), 6.81 (s, 1H), 6.76 (d, J = 8.6 Hz, 1H), 4.56 (t, J = 6.6 Hz, 2H), 4.09 (s, 3H), 3.48 (m, 4H), 2.37 (m, 2H), 2.24 (m, 4H), 1.96 (m, 2H). ^{13}C NMR (100 MHz, DMSO-d_6) δ 158.55, 152.96, 147.63, 142.36, 140.84, 139.55, 133.48, 132.67, 131.32, 128.32, 126.71, 125.63, 125.39, 124.37, 124.13, 123.85, 123.39, 118.96, 117.25, 116.88, 116.65, 112.99, 108.15, 87.40, 66.53, 55.35, 53.78, 44.21, 38.32, 23.67. HRMS m/z: calcd for $C_{33}H_{34}N_3O_2S^+$ [M-I]$^+$ 536.23662; found 536.23564 [M-I]$^+$. HPLC analysis: retention time at 2.827 min eluted with MeOH/H_2O = 50:50 v/v, purity = 97%.

Compound **(3)**: *2-((E)-4-(dimethylamino)styryl)-1-methyl-4-((Z)-(3-(3-morpholinopropyl)benzo[d]thiazol-2(3H)-ylidene)methyl)quinolin-1-ium iodide* was obtained as a brown solid with 68% yield. ^{1}H NMR (400 MHz, DMSO-d_6) δ 8.62 (d, J = 8.3 Hz, 1H), 8.13 (d, J = 8.8

Hz, 1H), 8.04 (s, 1H), 7.97 (dd, *J* = 16.8, 8.4 Hz, 2H), 7.79 (d, *J* = 8.8 Hz, 2H), 7.75 – 7.70 (m, 2H), 7.67 (s, 1H), 7.58 (dd, *J* = 16.8, 8.4 Hz, 2H), 7.45 (s, 1H), 7.36 (t, *J* = 7.6 Hz, 1H), 7.27 (d, *J* = 8.8 Hz, 1H), 6.86 – 6.76 (m, 3H), 4.60 (t, J = 6.6 Hz, 2H), 4.13 (s, 3H), 3.49 (m, 4H), 3.05 (s, 6H), 2.39 (m, 2H), 2.27 (m, 4H), 1.99 (s, 2H). ^{13}C NMR (100 MHz, DMSO-d_6) δ 158.36, 153.25, 152.33, 147.66, 142.88, 140.95, 139.64, 133.45, 130.97, 130.61, 125.41, 124.31, 124.08, 123.91, 123.16, 120.37, 119.01, 115.16, 112.95, 112.20, 108.14, 87.29, 66.53, 55.37, 53.79, 38.31, 23.67. HRMS m/z: calcd for $C_{35}H_{39}N_4OS^+$ $[M\text{-}I]^+$ 563.2839; found 563.2875 $[M\text{-}I]^+$. HPLC analysis: retention time at 2.794 min eluted with MeOH/H_2O = 50:50 v/v, purity = 97%.

Compound **(4)**: *2-((E)-4-(diphenylamino)styryl)-1-methyl-4-((Z)-(3-(3-morpholinopropyl)benzo[d]thiazol-2(3H)-ylidene)methyl)quinolin-1-ium iodide* was obtained as a brown solid with 58% yield. ^{1}H NMR (400 MHz, DMSO-d_6) δ 8.58 (d, *J* = 8.4 Hz, 1H), 8.04 (d, *J* = 8.8 Hz, 1H), 8.00 (d, *J* = 7.9 Hz, 1H), 7.88 (d, *J* = 7.8 Hz, 1H), 7.79 (d, *J* = 8.7 Hz, 2H), 7.65 (dd, *J* = 8.0, 3.6 Hz, 2H), 7.52 (m, 2H), 7.50 (s, 1H), 7.35 – 7.30 (m, 5H), 7.10 (m, 3H), 7.04 (d, *J* = 7.6 Hz, 4H), 6.90 (d, *J* = 8.7 Hz, 2H), 6.79 (s, 1H), 4.55 (t, *J* = 6.4 Hz, 2H), 4.04 (s, 3H), 3.40 (s, 4H), 2.31 (t, *J* = 6.2 Hz, 2H), 2.17 (s, 4H), 1.94 – 1.87 (m, 2H). ^{13}C NMR (100 MHz, DMSO-d_6) δ 159.06, 152.59, 149.69, 147.88, 146.81, 141.06, 140.82, 139.49, 133.60, 130.55, 130.29, 128.90, 125.54, 124.77, 124.50, 124.27, 123.86, 123.50, 121.57, 121.50, 119.39, 118.99, 113.18, 108.30, 87.76, 66.51, 55.34, 53.76, 44.34, 38.52, 23.71. HRMS m/z: calcd for $C_{45}H_{43}N_4OS^+$ $[M\text{-}I]^+$ 687.31521; found 687.31510 $[M\text{-}I]^+$. HPLC analysis: retention time 2.862 min eluted with MeOH/H_2O = 50:50 v/v, purity > 99%.

Compound **(5)**: *2-((E)-4-cyanostyryl)-1-methyl-4-((Z)-(3-(3-morpholinopropyl)benzo[d]thiazol-2(3H)-ylidene)methyl)quinolin-1-ium iodide* was obtained as a brown solid with 64% yield. ^{1}H NMR (600 MHz, DMSO-d_6) δ 8.68 (d, *J* = 8.3 Hz, 1H), 8.13 (m, 3H), 8.06 (d, *J* = 7.8 Hz, 1H), 8.01 – 7.92 (m, 4H), 7.76 (m, 2H), 7.68 (d, *J* = 8.3 Hz, 1H), 7.59 (m, 2H), 7.40 (t, *J* = 7.6 Hz, 1H), 6.94 (s, 1H), 4.66 (t, *J* = 6.6 Hz, 2H), 4.13 (s, 3H), 3.45 (s, 4H), 2.38 (t, *J* = 6.0 Hz, 2H), 2.23 (s, 4H), 1.99 (dt, *J* = 12.7, 6.2 Hz, 2H). ^{13}C NMR (100 MHz, DMSO-d_6) δ 159.99, 151.53, 148.32, 140.79, 140.13, 139.51, 138.89, 133.86, 133.22,

129.46, 128.53, 127.14, 125.93, 125.59, 124.90, 124.45, 123.93, 123.51, 119.18, 119.06, 113.55, 112.33, 108.61, 88.49, 66.49, 55.33, 53.76, 44.52, 38.69, 30.73, 23.79. HRMS m/z: calcd for $C_{34}H_{33}N_4OS^+$ [M-I]$^+$ 545.2370; found 545.2362 [M-I]$^+$. HPLC analysis: retention time 2.881 min eluted with MeOH/H_2O = 50:50 v/v, purity = 99%.

Compound **(6)**: *1-methyl-4-((Z)-(3-(3-(4-methylpiperidin-1-yl)propyl)benzo[d]thiazol-2(3H)-ylidene)methyl)-2-((E)-4-(methylthio)styryl)quinolin-1-ium iodide* was synthesized according to the procedures reported previously.[50] The compound was obtained as a dark brown solid with 59% yield. ^{1}H NMR (400 MHz, DMSO-d_6) δ 8.68 (s, 1H), 8.16 (m, 1H), 8.06 (m, 1H), 8.01 – 7.96 (m, 1H), 7.88 (d, J = 8.2 Hz, 2H), 7.77 – 7.70 (m, 3H), 7.63 (m, 2H), 7.60 – 7.56 (m, 1H), 7.39 (m, 3H), 6.90 (s, 1H), 4.63 (m, 2H), 4.15 (s, 3H), 2.56 (s, 3H), 2.00 (m, 4H), 1.50 (m, 3H), 1.22 (m, 6H), 0.85 (m, 3H). ^{13}C NMR (100 MHz, DMSO-d_6) δ 159.36, 152.45, 148.28, 142.09, 140.88, 139.54, 133.71, 132.09, 130.11, 129.43, 128.43, 126.97, 126.07, 124.69, 124.32, 123.98, 123.49, 120.95, 119.07, 113.23, 108.50, 87.95, 72.97, 63.55, 38.59, 35.59, 34.06, 31.76, 29.17, 27.02, 25.58, 22.57, 14.78. HRMS m/z: calcd for $C_{36}H_{40}N_3S_2^+$ [M-I]$^+$ 578.265; found 578.265 [M-I]$^+$. HPLC analysis: retention time 2.806 min eluted with MeOH/H_2O = 50:50 v/v, purity = 97%.

Compound **(7)**: *2-((E)-4-hydroxystyryl)-1-methyl-4-((Z)-(3-(3-(4-methylpiperidin-1-yl)propyl)benzo[d]thiazol-2(3H)-ylidene)methyl)quinolin-1-ium iodide* was synthesized according to the procedures reported previously.[50] The compound was obtained as a dark brown solid with 62% yield. ^{1}H NMR (400 MHz, DMSO-d_6) δ 10.14 (s, 0.79H), 8.71 (s, 1H), 8.19 (d, J = 8.5 Hz, 1H), 8.08 (d, J = 8.5 Hz, 1H), 8.01 – 7.98 (t, J = 7.7 Hz, 1H), 7.83 (d, J = 8.5 Hz, 2H), 7.75 (t, J = 7.7 Hz, 2H), 7.68 (s, 1H), 7.65 – 7.54 (m, 4H), 7.39 (t, J = 7.7 Hz, 1H), 6.93 – 6.86 (m, 3H), 4.64 (m, 2H), 4.17 (s, 3H), 2.14 (m, 2H), 1.75 – 1.57 (m, 3H), 1.22 (m, 6H), 0.88 (m, 5H). ^{13}C NMR (100 MHz, DMSO-d_6) δ 160.41, 158.93, 153.07, 148.37, 143.56, 142.05, 140.63, 139.58, 133.69, 131.12, 130.11, 130.03, 128.46, 126.87, 124.62, 124.21, 124.02, 123.56, 119.11, 118.20, 116.32, 112.97, 108.60, 87.59, 52.53, 52.31, 43.75, 38.60, 34.04,

30.75, 29.46, 22.57. HRMS m/z: calcd for $C_{35}H_{38}N_3OS^+$ $[M-I]^+$ 548.273; found 548.274 $[M-I]^+$. HPLC analysis: retention time 2.789 min eluted with MeOH/H_2O = 50:50 v/v, purity = 98%.

Compound **(8)**: *2-((E)-4-(dimethylamino)styryl)-1-methyl-4-((Z)-(3-(3-(4-methylpiperidin-1-yl)propyl)benzo[d]thiazol-2(3H)-ylidene)methyl)quinolin-1-ium iodide* was synthesized according to the procedures reported previously.[50] The compound was obtained as a dark brown solid with 63% yield. ^{1}H NMR (400 MHz, DMSO-d_6) δ 8.66 (s, 1H), 8.13 (m, 1H), 8.04 (m, 1H), 7.97 – 7.93 (m, 1H), 7.80 (d, J = 8.4 Hz, 2H), 7.73 – 7.68 (m, 2H), 7.62 (s, 1H), 7.55 (d, J = 7.8 Hz, 1H), 7.44 (m, 1H), 7.39 – 7.33 (m, 2H), 6.83 (s, 1H), 6.79 (d, J = 8.7 Hz, 2H), 4.60 (m, 2H), 4.14 (s, 3H), 3.04 (s, 6H), 2.00 (m, 2H), 1.60 (m, 5H), 1.22 (m, 6H), 0.87 (m, 3H). ^{13}C NMR (100 MHz, DMSO-d_6) δ 158.27, 153.30, 152.34, 139.62, 133.48, 131.03, 130.11, 128.34, 126.73, 124.36, 124.10, 123.96, 123.46, 123.14, 118.99, 115.10, 112.19, 87.24, 72.97, 63.55, 38.38, 31.75, 29.05, 27.02, 22.56, 14.43. HRMS m/z: calcd for $C_{37}H_{43}N_4S^+$ $[M-I]^+$ 575.320; found 575.321 $[M-I]^+$. HPLC analysis: retention time 2.796 min eluted with MeOH/H_2O = 50:50 v/v, purity = 96%.

Compound **(9)**: *2-((E)-4-(diphenylamino)styryl)-1-methyl-4-((Z)-(3-(3-(4-methylpiperidin-1-yl)propyl)benzo[d]thiazol-2(3H)-ylidene)methyl)quinolin-1-ium iodide* was obtained as a brown solid with 73% yield. ^{1}H NMR (400 MHz, DMSO-d_6) δ 8.78 (s, 1H), 8.20 (s, 1H), 8.05 (m, 2H), 7.82 (m, 4H), 7.65 (m, 3H), 7.42 (m, 6H), 7.15 (m, 6H), 7.01 (m, 2H), 6.89 (s, 1H), 4.68 (m, 2H), 4.19 (s, 3H), 2.20 (m, 3H), 1.77 (m, 2H), 1.24 (m, 6H), 0.92 (m, 5H). ^{13}C NMR (100 MHz, DMSO-d_6) δ 158.93, 152.91, 149.74, 148.40, 146.81, 141.40, 140.47, 139.56, 133.75, 130.56, 130.31, 130.22, 128.85, 128.53, 127.03, 125.92, 125.59, 125.24, 124.75, 124.13, 123.60, 121.57, 119.21, 112.94, 108.87, 87.64, 52.82, 43.34, 38.67, 31.73, 29.50, 28.45. HRMS m/z: calcd for $C_{47}H_{47}N_4S^+$ $[M-I]^+$ 699.35159; found 699.35101 $[M-I]^+$. HPLC analysis: retention time 2.829 min eluted with MeOH/H_2O = 50:50 v/v, purity > 99%.

Compound **(10)**: *2-((E)-4-cyanostyryl)-1-methyl-4-((Z)-(3-(3-(4-methylpiperidin-1-yl)propyl)benzo[d]thiazol-2(3H)-ylidene)methyl)quinolin-1-ium iodide* was obtained as a brown solid with 68% yield. ^{1}H NMR (400 MHz, DMSO-d_6) δ 8.79 – 8.62 (d, J = 8.1 Hz, 1H), 8.16 (m, 2H), 8.08 –

7.98 (m, 3H), 7.78 (m, 5H), 7.62 (m, 3H), 7.47 – 7.36 (m, 2H), 6.97 (d, J = 8.1 Hz, 1H), 4.67 (m, 2H), 4.17 (s, 3H), 2.13 – 1.71 (m, 6H), 1.56 – 1.39 (m, 3H), 1.31 – 1.22 (m, 2H), 0.83 (m, 4H). ^{13}C NMR (100 MHz, DMSO) δ 159.97, 153.11, 151.75, 148.83, 141.39, 140.41, 140.09, 139.52, 139.09, 134.41, 133.97, 133.23, 129.48, 128.63, 127.31, 126.52, 125.90, 125.01, 124.44, 124.06, 123.69, 119.85, 119.53, 119.13, 113.24, 112.40, 109.08, 105.44, 88.27, 52.63, 38.91, 38.68, 34.09, 30.35, 21.88. HRMS m/z: calcd for $C_{36}H_{37}N_4S^+$ $[M\text{-}I]^+$ 557.27334; found 557.27428 $[M\text{-}I]^+$. HPLC analysis: retention time 2.901 min eluted with MeOH/H_2O = 50:50 v/v, purity = 97%.

UV-Vis and fluorescence assays. UV-vis spectra were obtained by using Lambda 25 Spectrophotometer (Perkin Elmer), compounds (5 μM) were dissolved in Tris-HCl buffer (10 mM, pH 7.4) containing KCl (60 mM), and different nucleic acids (Ds26, Pu27, Htg24) were added slowly until the titration was saturated. The fluorescence spectrum was recorded on a LS-45 fluorescence spectrometer (Perkin Elmer), the colorimetric dish has a slit width of 1 mm and an optical diameter of 10 mm, compounds (5 μM) were dissolved in Tris-HCl buffer (10 mM, pH 7.4) containing KCl (60 mM), and different nucleic acids (double stranded or single stranded or G4-DNA) were added slowly until the titration was saturated. The detection limit (LOD) was calculated by fluorescence titration according to the formula LOD = K (S_b/m). According to the International Union of Pure and Applied Chemistry (IUPAC), K value is taken as 3 generally. S_b is the standard deviation of blank multiple measurements (n = 20) and m is the slope of calibration curve, which indicates the sensitivity of the method.[51] The binding constants were analyzed by applying an independent site model using nonlinear fitting with the following equation: $F/F_0=1+(Q-1)/2\{N+1+X-[(X+1+N)^2-4X]^{1/2}\}$. Where F_0 is the fluorescence intensity of **1-10** without the addition of DNA, F_{max} is the fluorescence intensity at the saturation of DNA, $Q=F_{max}(F_0)^{-1}$, $N=(K_{eq}\text{Cdye})^{-1}$, $X=nC_{DNA}(C_{dye})^{-1}$ and n is a putative number of binding sites on a given DNA matrix. All data were collected and plotted with Origin 9.0.

Measurement of fluorescent quantum yields of compounds 1-10. The fluorescence quantum yields of various ligands and DNA were calculated according to the standard of fluorescein (Φ = 0.95) in the

condition of 1% NaOH ethanol.[52] Five gradient increasing solutions were added to the fixed concentration of DNA solution, and the UV absorption value and fluorescence intensity value of each gradient concentration compound and DNA were recorded. The fluorescence quantum yield was calculated according to the equation: $\Phi_X = \Phi_{ST} (Grad_X / Grad_{ST}) (\eta^2_X / \eta^2_{ST})$;[53] where the subscript ST is the standard and the subscript X is the test sample; Φ represents the fluorescence quantum yield value; Grad is the slope of the curve with the integrated fluorescence intensity as the ordinate, the ultraviolet absorbance as the abscissa, and η is the refractive index of the solvent used.

Circular dichroism (CD) measurements. The CD spectrum was measured by Chirascan spectrophotometer (Applied photophysics). A Tris-HCl (10 mM, pH = 7.4) containing 60 mM KCl was used to prepare the solutions of G4-DNA and ligands at 5 μM concentration. A quartz cuvette with a path length of 1 mm was used for the spectral measurements in the wavelength range of 220–340 nm with a bandwidth of 1 nm, a step of 1 nm and a point of 0.5 s/point. The CD spectral data were obtained by the average value of three scans. In addition, A concentration of G4-DNA at 5 μM was also prepared with the Tris-HCl (10 mM) containing 60 mM KCl at pH = 7.4. The compounds were added to the mixture for CD melting measurement. The data were recorded at an interval of 1 °C in the range of 25–95 °C with a heating rate of 1.0 °C/min. Origin 9.0 was used for final analysis of the data.

Fluorescence microscopy imaging study and cell staining effects. Fluorescence images obtained in U87 cells (human prostate cancer cells, ATCC® HTB-14) were recorded with a confocal laser scanning microscopy (ZEISS LSM 800 with Airscan). The nucleus localization reference dye, 6-diamidino-2-phenylindole (DAPI, 1 μM), was used with ligand **3**. The excitation wavelength of DAPI was set at 402 nm and that of ligand **3** was set at 488 nm or 571 nm. In the experiments, the compounds were able to enter the cell quickly without damaging the cell activity.

Cell imaging treated with RNase and DNase. U87 cells (human prostate cancer cells, ATCC® HTB-14) was cultured on a confocal dish for 24 h. Before dyeing experiments, it was precooled with methanol

at -4 °C for 2 min and then washed twice with PBS (10 mM). In order to make the cell membrane permeable, the U87 cells were cultured with 1% Triton X-100 for 15 min and then were washed with PBS thrice. The pretreated U87 cells were then stained with ligand **3** (5 μM) at 25 °C for 20 min. After washing with PBS for three times, one culture dish was treated with 100 ug/ml RNase (37 °C, 2 h) and the other was treated with 100 ug/ml DNase (37 °C, 2 h). Imaging experiments were then carried out on a Zeiss LSM800 confocal laser scanning microscope.

Immunofluorescence experiments. Confocal images of U87 cells stained with **3** and BG4: Cells grown on a glass dish were fixed in 4% paraformaldehyde/PBS for 15 min and followed it was infiltrated with 0.1% Triton-X 100/PBS at 37 °C for 30 min. Then, it was blocked with 5% goat serum/PBS at 37 °C for 3 h. Immunofluorescence tests were conducted by following the standard methods. Briefly, the glass dishes were incubated with Anti-DNA/RNA G-quadruplex (and related small molecules) [BG4] (Ab00174-1.1, Absolute) for 3 h at 37 °C. The glass dishes were washed six times with blocking buffer and then incubated with DyLight™ 405 AffiniPure Goat Anti-Mouse IgG (H+L) (115-475-062, Jackson) for 3 h at 37 °C. The glass dish was washed again with blocking buffer six times and then incubated with 5 μM **3** for 30 min. Finally, digital images were recorded using a ZEISS LSM 800 microscope and analyzed using ZEN software.

NMR Spectroscopy. Before taking measurements, the oligomeric DNA with a concentration of 300 μM was dissolved in phosphate buffer (25 mM KH_2PO_4, 10% D_2O, 70 mM KCl, pH = 7.4) and was heated to 95 °C, then annealed to room temperature and incubated for 24 h. During the measurement, **3** with a concentration of 150–450 μM were gradually added to the DNA solution for ^{1}H NMR experiment. The titration experiments were carried out at 25 °C on a 600 MHz spectrometer (Bruker).

PCR stop assay. The polymerase stop assays were conducted using a modified protocol of a previous report.[54] Briefly, the PCR stop assays were performed by addition of ligand at different concentrations (0–20 μM) to a 25 μl solution containing 1X PCR buffer, 2 μM of each oligomer, 0.16 μM dNTP and 2.5 U Taq polymerase (Invitrogen, USA). The concentration of the DNA (Htg24 or mutant) used in the

assays was 5 μM. Reaction mixtures were then incubated in a thermocycler by applying the following cycling conditions: 94 °C for 5 min followed by 30 cycles of 94 °C for 30 s, 56 °C for 30 s and 72 °C for 30 s. The amplified products were resolved on 15% polyacrylamide gel and were stained with SYBR Gold (Invitrogen, USA).

RNA isolation and qRT-PCR. HeLa cells (Human cervical cancer, ATCC® CRM-CCL-2) were seeded in six-well plates and were treated with different concentrations of compounds. After that, HeLa cells were further incubated for 36 h and followed to discard the culture medium. The six-well plate was then washed with 4 °C PBS for three times. After that, 0.5 ml Trizol (Sigma-Aldrich) was added to dissolve the cells for 3 min and then 0.2 ml chloroform was added. After the mixture was well shaken, the plate was allowed to stand for 3 min and followed by centrifugation at 13500 rpm at 4 °C for 15 min to separate the RNA-containing aqueous phase. Total RNA was precipitated from the aqueous phase with anhydrous isopropanol. The RNA precipitate was washed with 75% ethanol (containing 25% DEPC water) and then was dissolved in 20 μl of RNase-free redistilled water. In order to remove the genomic DNA contamination in the isolated RNA, the samples were treated with DNase I and identified by polymerase chain reaction. The prepared RNA is therefore contained no genomic DNA. Then, the HiScript® II One Step qRT-PCR SYBR Green Kit was used for reverse transcription of RNA and quantitative analysis of transcribed cDNA. The concentration of RNA is 0.5–2 μg per reaction. The forward and reverse primer sequences (hTERC) for telomerase amplification are 5′-GCCTTCCACCGTTCATTCTA-3′ and 5′-CTGACAGAGCCCAACTCTTC-3′ and the forward and reverse primer sequences (hTERT) for telomerase amplification are 5′-CGTGGTTTCTGTGTGGTGTC-3′ and 5′-TGGAACCCAGAAAGATGGTC-3′. GAPDH was used as an internal control for normalization and the internal control GAPDH is amplified by the forward primer 5′-GGGAAACTGTGGCGTGAT-3′ and the reverse primer 5′-GAGTGGGTGTCGCTGTTGA-3′. The RNA was reverse transcripted and amplified by qRT-PCR (analytikjena, qTOWER2.2). A comparative Ct (ΔΔCT) method was used to compare the mRNA expression levels of genes of interest.

Relative telomere length determination. HeLa cells (Human cervical cancer, ATCC® CRM-CCL-2) were inoculated into a 6-well plate and treated with different concentrations of compound **3** for 18 days. After digestion, cells were centrifuged and re-suspended in PBS solution to collect cells twice. Then, DNA extract (10 mmol/L Tris HCl, 0.1 mol/L EDTA, 0.5% SDS) and protease K (100 μg/ml) were added and incubated at 50 ℃ for 3 h. Then, the solution was extracted with phenol, phenol/chloroform/isoamyl alcohol and followed with chloroform/isoamyl alcohol. The supernatant was collected after centrifugation at 2500 r/min. Then, to the supernatant 5 mol/L LiCl was added and centrifuged at 2500 r/min after 10 min ice bath. Isopropanol was added to the supernatant collected and then incubated at room temperature for 10 min. The precipitates were collected by centrifugation at 2500 r/min. To the precipitates a solution of 3 mol/L sodium acetate and the absolute ethanol precooled at -20 ℃ were successively added. The precipitated DNA was collected by centrifugation at 12000 r/min. The precipitated DNA was then stored in an appropriate amount of solution (10 mmol/L Tris HCl, 0.01 mol/L EDTA). The Maxima SYBR Green qPCR Master Mix (2x) (Thermo Scientifific), Nuclease-free water and primer sequences (Thermo Scientifific) were used for relative telomere length determination. The concentration of gDNA is 0.5–10 ng per reaction. The primer sequences (Tel-F) are 5′-GGTTTTTGAGGGTGAGGGTGAGGGTGAGGGTGAGGGT-3′ and (Tel-R) 5′-TCCCGACTATCCCTATCCCTATCCCTATCCCTATCCCTA-3′. hRPLPO was used as an internal control, the internal control hRPLPO was amplified by the primer (hRPLPO-F) 5′-CCCATTCTATCATCAACGGGTACAA-3′ and the primer (hRPLPO-R) 5′-CAGCAAGTGGGAAGGTGTAATCC-3′. The gDNA was amplified by qRT-PCR (analytikjena, qTOWER2.2). A comparative Ct (ΔΔCT) method was used to estimate the relative telomere length by the determination of gDNA.

Telomerase activity assays. The HeLa cells after being treated with ligand **3** at different concentrations for 36 hours, 10^6 cells were re-suspended in 200 μl CHAPS lysis buffer and incubated on ice for 30 min. The same operation for positive control cells was also performed. Then, all the supernatants were

transferred to aseptic enzyme free test tube and the protein concentration was determined with BCA Kit (biyuntian). The protein at 10–750 ng/ml in the cell extract were incubated with TRAP buffer (20 mM Tris–HCl, pH 8.3, containing 1.5 mM $MgCl_2$, 63 mM KCl, 0.05% (v/v) Tween 20, 1 mM EGTA, and 0.01% BSA) supplemented with dNTP mixture, 100 ng/μl TS primer mixture (5′-AAT CCG TCG AGC AGA GTT-3′), TRAP primer mixture (containing 100 ng/μl ACX (5′-GCGCGGCTTACCCTTACCCTTACCCTAACC-3′), 100 ng/μl NT (5'-ATCGCTTCTCGGCCTTTT-3') and 0.01 amol/μl TSNT (5'-AATCCGTCGAGCAGAGTTAAAAGGCCGAGAAGCGAT-3')), ddH_2O, Taq polymerase (Takara). Telomerase was extended in 30 ℃ water bath for 30 minutes and inactivated at 95 ℃ for 2 min. PCR was performed at 94 ℃ for 30 s, 59 ℃ for 30 s, 72 ℃ for 1 min for 33 cycles and 72 ℃ for 5 min in a thermocycler (Bioer). PCR samples were separated on a 10% (w/v) native-PAGE gel in 0.5xTBE for 2 h at 120 V. After electrophoresis, the gel was stained with SYBR Gold for 30 min at room temperature.

***β*-Galactosidase (SA-*β*-gal) staining of cell senescence.** HeLa cells (Human cervical cancer, ATCC® CRM-CCL-2) were inoculated in a 6-well plate and were treated with the compound different concentrations. After that, the HeLa cells were further incubated for 18 days. The medium containing different concentrations of compound was added every three days. Then, the medium was discarded and the cells were washed with PBS for 3 times. The *β*-galactosidase staining fixative was added and fixed at room temperature for 15 min. Then, the cell fixative was removed and washed three times with PBS for 3 min each time. After that, the working solution of *β*-galactosidase staining was added and incubated at 37 °C overnight. Then, the data were observed and collected under an inverted fluorescence microscope (Olympus IX71).

Cytotoxicity test. The cancer cells such as U87 cells were inoculated in a 96-well plate and cultured in 37 °C and 5% CO_2. The DMEM medium containing 10% fetal bovine serum and 0.5% bivalent antibody was used. After 48 h, the 96-well plate was removed and washed three times with the pre-cooled PBS. DMEM complete medium containing different gradient ligand such as **3** was added. The culture was

continued at 37 °C and 5% CO_2 for 36 h. After removing the medium from the 96-well plate, 200 μl of 5 mg/ml MTT solution was added to each well and then the 96-well plate was keeping away from light for 4 h. After that, the MTT solution was removed; DMSO 100 μl was added to the plate; and the deck adhering to 96-well plate was fully dissolved. The 96-well plate was transferred to the enzyme label and its absorbance was measured at 577 nm. Finally, the cell survival rate was determined according to the absorbance value.

Isothermal titration calorimetry (ITC) measurements of ligand-DNA interactions. ITC experiments were carried out in MicroCal PEAQ-ITC (Malvern, USA) microcalorimeter. DNA sequences were pre-annealed in 25 mM KH_2PO_4, 60 mM KCl buffer (pH 7.4, containing 0.5% (v/v) DMSO) by heated to 95 °C in water bath for 5 min. Then, it was cooled to 25 °C and placed at 4 °C overnight. The pre-annealed DNA sequences (10 μM) in buffer was kept in the sample cell and the ligands (500 μM) were filled in the syringe of a volume 40 μl in the same buffer. The ligand was mixed with the sample by stirring the syringe at 750 rpm at 25 °C. There were 19 injections with a duration of 4 s and an interval of 150 s. Under the same conditions, the ligand was injected into the cells containing only buffer solution for a blank titration. The heat generated by the interaction was determined by subtracting the blank heat from the heat of ligand DNA titration. Finally, the corrected data are fitted into the appropriate binding model to obtain the binding enthalpy.

Statistical analysis. All assays were performed in three independent experiments (technical triplicates). Statistical calculations for bioassays were performed using GraphPad Prism 5.0 software. All results are expressed as means ± SD. The criterion for statistical significance was taken as ns: $p>0.05$, *$p<0.05$, **$p<0.01$, ***$p<0.001$. In the cell proliferation assays, data were analyzed with GraphPad Prism 5 software to determine IC_{50} (concentration at 50% cell viability) using sigmoidal dose–response analysis, with variable fitting for top, bottom, and slope.

ASSOCIATED CONTENT

Supporting Information:

The Supporting Information is available including:

Sequences of oligonucleotides used for assays, Spectroscopic data of ligands and their binding properties, Fluorescence titration assays, Equilibrium binding constants, Circular dichroism measurements, Gel electrophoresis experiments, Isothermal titration calorimetry experiments, qRT-PCR assays, HPLC purity of final compounds, ^{1}H NMR and ^{13}C NMR spectra of final compounds (PDF).

Molecular string files for all of the final target compounds (CSV)

AUTHOR INFORMATION

Corresponding Authors

Kun Zhang − School of Biomedical and Pharmaceutical Sciences, Guangdong University of Technology, Guangzhou 510006, P. R. China; School of Biotechnology and Health Sciences, Wuyi University, Jiangmen, 529020, P.R. China; Email: kzhang@gdut.edu.cn

Wing-Leung Wong − State Key Laboratory of Chemical Biology and Drug Discovery, Department of Applied Biology Chemical Technology, The Hong Kong Polytechnic University, Hung Hom, Kowloon, Hong Kong, China; School of Biotechnology and Health Sciences, Wuyi University, Jiangmen, 529020, P. R. China; orcid.org/0000-0001-7191-7578; Email: wing.leung.wong@polyu.edu.hk

Yu-Jing Lu − School of Biomedical and Pharmaceutical Sciences, Guangdong University of Technology, Guangzhou 510006, P. R. China; Engineering Research Academy of High Value Utilization of Green Plants, Meizhou 514779, P. R. China; Email: luyj@gdut.edu.cn

Authors

Wei Long − School of Biomedical and Pharmaceutical Sciences, Guangdong University of Technology, Guangzhou 510006, P. R. China.

Bo-Xin Zheng − School of Biomedical and Pharmaceutical Sciences, Guangdong University of Technology, Guangzhou 510006, P. R. China.

Xuan-He Huang − School of Biomedical and Pharmaceutical Sciences, Guangdong University of Technology, Guangzhou 510006, P. R. China.

Meng-Ting She − School of Biomedical and Pharmaceutical Sciences, Guangdong University of Technology, Guangzhou 510006, P. R. China.

Ao-Lu Liu − School of Biomedical and Pharmaceutical Sciences, Guangdong University of Technology, Guangzhou 510006, P. R. China

Notes

The authors declare no competing financial interest

ACKNOWLEDGMENTS

This work was supported by the National Natural Science Foundation of China (81473082, 22077020), Natural Science Foundation of Guangdong Province, China (2017A030313078, 2017A030313071 and 2019A1515011799). Jiangmen Program for Innovative Research Team (No.: 2018630100180019806), the Department of Education of Guangdong Province, China (2016KCXTD005 and 2017KSYS010), and the Department of Agriculture and Rural Affairs of Guangdong Province, China (2018LM2175). We also acknowledge Dr. Shan-Yue Guan (Instrumental Analysis & Research Center, Sun Yat-sen University), Dr. Zhi-Shu Huang and Dr. Shuo-Bin Chen (School of Pharmaceutical Sciences, Sun Yat-sen University) for their assistance on the NMR experiments of molecular interaction study.

ABBREVIATIONS

$TMPyP_4$, 5,10,15,20-tetrakis(*N*-methyl-4-pridyl)porphyrine; PDC-360A, (2,6-*N,N′*-methyl-quinolinio-3-yl)-pyridine dicarboxamide [methyl-3H]; Se2SAP, 5,10,15,20-[tetra(N-methyl-3-pyridyl)]-26,28-diselenasapphyrin chloride; Phen-DC3, 3,3'-((1,10-phenanthroline-2,9-dicarbonyl)bis(azanediyl))bis(1-methylquinolin-1-ium); BRACO19, *N,N′*-(9-((4-(dimethylamino)phenyl)amino)acridine-3,6-diyl)bis(3-(pyrrolidin-1-yl)propanamide); CND-1, cyclic naphthalene diimide-1; DAPI, 4′,6-diamidino-2-phenylindole; TO, thiazole orange; ISTO, isaindigotone skeleton thiazole orange; TOPI, TO-based protein identifier; PyroTASQ, pyrene template-assembled synthetic G-quartets.

REFERENCES

(1) Simonsson, T. G-quadruplex DNA structures - variations on a theme. *Biol. Chem.* **2001**, *382*, 621–628.

(2) Bochman, M. L.; Paeschke, K.; Zakian, V. A. DNA secondary structures: stability and function of G-quadruplex structures. *Nat. Rev. Genet.* **2012**, *13*, 770–780.

(3) Biffi, G.; Tannahill, D.; McCafferty, J.; Balasubramanian, S. Quantitative visualization of DNA G-quadruplex structures in human cells. *Nat. Chem.* **2013**, *5*, 182–186.

(4) Di Antonio, M.; Ponjavic, A.; Radzevicius, A.; Ranasinghe, R. T.; Catalano, M.; Zhang, X. Y.; Shen, J. Z.; Needham, L. M.; Lee, S. F.; Klenerman, D.; Balasubramanian, S. Single-molecule visualization of DNA G-quadruplex formation in live cells. *Nat. Chem.* **2020**, *12*, 832–837.

(5) Izbicka, E.; Wheelhouse, R. T.; Raymond, E.; Davidson, K. K.; Lawrence, R. A.; Sun, D. Y.; Windle, B. E.; Hurley, L. H.; Von Hoff, D. D. Effects of cationic porphyrins as G-quadruplex interactive agents in human tumor cells. *Cancer Res.* **1999**, *59*, 639–644.

(6) Phan, A. T.; Modi, Y. S.; Patel, D. J. Propeller-type parallel-stranded G-quadruplexes in the human c-MYC promoter. *J. Am. Chem. Soc.* **2004**, *126*, 8710–8716.

(7) Chen, Z. F.; Qin, Q. P.; Qin, J. L.; Liu, Y. C.; Huang, K. B.; Li, Y. L.; Meng, T.; Zhang, G. H.; Peng,

Y.; Luo, X. J.; Liang, H. Stabilization of G-quadruplex DNA, inhibition of telomerase activity, and tumor cell apoptosis by organoplatinum(II) complexes with oxoisoaporphine. *J. Med. Chem.* **2015**, *58*, 2159–2179.

(8) Neidle, S. Quadruplex nucleic acids as novel therapeutic targets. *J. Med. Chem.* **2016**, *59*, 5987–6011.

(9) Siddiqui-Jain, A.; Grand, C. L.; Bearss, D. J.; Hurley, L. H. Direct evidence for a G-quadruplex in a promoter region and its targeting with a small molecule to repress c-MYC transcription. *Proc. Natl. Acad. Sci. U.S.A.* **2002**, *99*, 11593–11598.

(10) Patel, D. J.; Phan, A. T.; Kuryavyi, V. Human telomere, oncogenic promoter and 5'-UTR G-quadruplexes: diverse higher order DNA and RNA targets for cancer therapeutics. *Nucleic Acids Res.* **2007**, *35*, 7429–7455.

(11) Lipps, H. J.; Rhodes, D. G-quadruplex structures: in vivo evidence and function. *Trends Cell Biol.* **2009**, *19*, 414–422.

(12) Paeschke, K.; Simonsson, T.; Postberg, J.; Rhodes, D.; Lipps, H. J. Telomere end-binding proteins control the formation of G-quadruplex DNA structures in vivo. *Nat. Struct. Mol. Biol.* **2005**, *12*, 847–854.

(13) Rhodes, D.; Lipps, H. J. G-quadruplexes and their regulatory roles in biology. *Nucleic Acids Res.* **2015**, *43*, 8627–8637.

(14) Moye, A. L.; Porter, K. C.; Cohen, S. B.; Phan, T.; Zyner, K. G.; Sasaki, N.; Lovrecz, G. O.; Beck, J. L.; Bryan, T. M. Telomeric G-quadruplexes are a substrate and site of localization for human telomerase. *Nat. Commun.* **2015**, *6*, 7643.

(15) Greider, C. W.; Blackburn, E. H. Identification of a specific telomere terminal transferase activity in tetrahymena extracts. *Cell* **1985**, *43*, 405–413.

(16) Gomez, D.; Aouali, N.; Londono-Vallejo, A.; Lacroix, L.; Megnin-Chanet, F.; Lemarteleur, T.; Douarre, C.; Shin-ya, K.; Mailliet, P.; Trentesaux, C.; Morjani, H.; Mergny, J. L.; Riou, J. F.

Resistance to the short term antiproliferative activity of the G-quadruplex ligand 12459 is associated with telomerase overexpression and telomere capping alteration. *J. Biol. Chem.* **2003**, *278*, 50554–50562.

(17) Sissi, C.; Palumbo, M. Telomeric G-quadruplex architecture and interactions with potential drugs. *Curr. Pharm. Design* **2014**, *20*, 6489–6509.

(18) Lipinska, N.; Romaniuk, A.; Paszel-Jaworska, A.; Toton, E.; Kopczynski, P.; Rubis, B. Telomerase and drug resistance in cancer. *Cell. Mol. Life Sci.* **2017**, *74*, 4121–4132.

(19) Oganesian, L.; Bryan, T. M. Physiological relevance of telomeric G-quadruplex formation: a potential drug target. *Bioessays* **2007**, *29*, 155–165.

(20) Tan, Z.; Tang, J.; Kan, Z. Y.; Hao, Y. H. Telomere G-quadruplex as a potential target to accelerate telomere shortening by expanding the incomplete end-replication of telomere DNA. *Curr. Top. Med. Chem.* **2015**, *15*, 1940–1946.

(21) Shin-ya, K.; Wierzba, K.; Matsuo, K.; Ohtani, T.; Yamada, Y.; Furihata, K.; Hayakawa, Y.; Seto, H. Telomestatin, a novel telomerase inhibitor from streptomyces anulatus. *J. Am. Chem. Soc.* **2001**, *123*, 1262–1263.

(22) Brooks, T. A.; Hurley, L. H. Targeting MYC expression through G-quadruplexes. *Genes Cancer* **2010**, *1*, 641–649.

(23) Seenisamy, J.; Bashyam, S.; Gokhale, V.; Vankayalapati, H.; Sun, D.; Siddiqui-Jain, A.; Streiner, N.; Shin-ya, K.; White, E.; Wilson, W. D.; Hurley, L. H. Design and synthesis of an expanded porphyrin that has selectivity for the c-MYC G-quadruplex structure. *J. Am. Chem. Soc.* **2005**, *127*, 2944–2959.

(24) Granotier, C.; Pennarun, G.; Riou, L.; Hoffschir, F.; Gauthier, L. R.; De Cian, A.; Gomez, D.; Mandine, E.; Riou, J. F.; Mergny, J. L.; Mailliet, P.; Dutrillaux, B.; Boussin, F. D. Preferential binding of a G-quadruplex ligand to human chromosome ends. *Nucleic Acids Res.* **2005**, *33*, 4182–4190.

(25) De Cian, A.; DeLemos, E.; Mergny, J. L.; Teulade-Fichou, M. P.; Monchaud, D. Highly efficient G-quadruplex recognition by bisquinolinium compounds. *J. Am. Chem. Soc.* **2007**, *129*, 1856–1857.

(26) Lombardo, C. M.; Martinez, I. S.; Haider, S.; Gabelica, V.; De Pauw, E.; Moses, J. E.; Neidle, S. Structure-based design of selective high-affinity telomeric quadruplex-binding ligands. *Chem. Commun.* **2010**, *46*, 9116–9118.

(27) Esaki, Y.; Islam, M. M.; Fujii, S.; Sato, S.; Takenaka, S. Design of tetraplex specific ligands: cyclic naphthalene diimide. *Chem. Commun.* **2014**, *50*, 5967–5969.

(28) Yaku, H.; Murashima, T.; Miyoshi, D.; Sugimoto, N. Anionic phthalocyanines targeting G-quadruplexes and inhibiting telomerase activity in the presence of excessive DNA duplexes. *Chem. Commun.* **2010**, *46*, 5740–5742.

(29) Nygren, J.; Svanvik, N.; Kubista, M. The interactions between the fluorescent dye thiazole orange and DNA. *Biopolymers* **1998**, *46*, 39–51.

(30) Lu, Y. J.; Yan, S. C.; Chan, F. Y.; Zou, L.; Chung, W. H.; Wong, W. L.; Qiu, B.; Sun, N.; Chan, P. H.; Huang, Z. S.; Gu, L. Q.; Wong, K. Y. Benzothiazole-substituted benzofuroquinolinium dye: a selective switch-on fluorescent probe for G-quadruplex. *Chem. Commun.* **2011**, *47*, 4971–4973.

(31) Yan, J. W.; Ye, W. J.; Chen, S. B.; Wu, W. B.; Hou, J. Q.; Ou, T. M.; Tan, J. H.; Li, D.; Cu, L. Q.; Huang, Z. S. Development of a universal colorimetric indicator for G-quadruplex structures by the fusion of thiazole orange and isaindigotone skeleton. *Anal. Chem.* **2012**, *84*, 6288–6292.

(32) Unger-Angel, L.; Rout, B.; Ilani, T.; Eisenstein, M.; Motiei, L.; Margulies, D. Protein recognition by bivalent, 'turn-on' fluorescent molecular probes. *Chem. Sci.* **2015**, *6*, 5419–5425.

(33) Laguerre, A.; Stefan, L.; Larrouy, M.; Genest, D.; Novotna, J.; Pirrotta, M.; Monchaud, D. A twice-as-smart synthetic G-quartet: PyroTASQ is both a smart quadruplex ligand and a smart fluorescent probe. *J. Am. Chem. Soc.* **2014**, *136*, 12406–12414.

(34) Lu, Y. J.; Deng, Q.; Hou, J. Q.; Hu, D. P.; Wang, Z. Y.; Zhang, K.; Luyt, L. G.; Wong, W. L.; Chow, C. F. Molecular engineering of thiazole orange dye: change of fluorescent signaling from universal to specific upon binding with nucleic acids in bioassay. *ACS Chem. Biol.* **2016**, *11*, 1019–1029.

(35) Lu, Y. J.; Deng, Q.; Hu, D. P.; Wang, Z. Y.; Huang, B. H.; Du, Z. Y.; Fang, Y. X.; Wong, W. L.; Zhang,

K.; Chow, C. F. A molecular fluorescent dye for specific staining and imaging of RNA in live cells: a novel ligand integration from classical thiazole orange and styryl compounds. *Chem. Commun.* **2015**, *51*, 15241–15244.

(36) Abdelhamid, M. A. S.; Gates, A. J.; Waller, Z. A. E. Destabilization of i-motif DNA at neutral pH by G-quadruplex ligands. *Biochemistry* **2019**, *58*, 245–249.

(37) Feigon, J.; Koshlap, K. M.; Smith, F. W. 1H NMR spectroscopy of DNA triplexes and quadruplexes. *Methods Enzymol.* **1995**, *261*, 225–255.

(38) Huang, Z. L.; Dai, J.; Luo, W. H.; Wang, X. G.; Tan, J. H.; Chen, S. B.; Huang, Z. S. Identification of G-quadruplex-binding protein from the exploration of RGG motif/G-quadruplex interactions. *J. Am. Chem. Soc.* **2018**, *140*, 17945–17955.

(39) Weinrich, S. L.; Pruzan, R.; Ma, L.; Ouellette, M.; Tesmer, V. M.; Holt, S. E.; Bodnar, A. G.; Lichtsteiner, S.; Kim, N. W.; Trager, J. B.; Taylor, R. D.; Carlos, R.; Andrews, W. H.; Wright, W. E.; Shay, J. W.; Harley, C. B.; Morin, G. B. Reconstitution of human telomerase with the template RNA component hTR and the catalytic protein subunit hTRT. *Nat. Genet.* **1997**, *17*, 498–502.

(40) Akincilar, S. C.; Low, K. C.; Liu, C. Y.; Yan, T. D.; Oji, A.; Ikawa, M.; Li, S.; Tergaonkar, V. Quantitative assessment of telomerase components in cancer cell lines. *Febs Lett.* **2015**, *589*, 974–984.

(41) Yokoi, S.; Yasui, K.; Iizasa, T.; Imoto, I.; Fujisawa, T.; Inazawa, J. TERC identified as a probable target within the 3q26 amplicon that is detected frequently in non-small cell lung cancers. *Clin. Cancer Res.* **2003**, *9*, 4705–4713.

(42) Cairney, C. J.; Keith, W. N. Telomerase redefined: integrated regulation of hTR and hTERT for telomere maintenance and telomerase activity. *Biochimie* **2008**, *90*, 13–23.

(43) Cayuela, M. L.; Flores, J. M.; Blasco, M. A. The telomerase RNA component TERC is required for the tumour-promoting effects of TERT overexpression. *Embo Rep.* **2005**, *6*, 268–274.

(44) Wu, K. J.; Grandori, C.; Amacker, M.; Simon-Vermot, N.; Polack, A.; Lingner, J.; Dalla-Favera, R.

Direct activation of TERT transcription by c-MYC. *Nat. Genet*. **1999**, *21*, 220–224.

(45) Flacco, A.; Ludovini, V.; Bianconi, F.; Ragusa, M.; Bellezza, G.; Tofanetti, F. R.; Pistola, L.; Siggillino, A.; Vannucci, J.; Cagini, L.; Sidoni, A.; Puma, F.; Varella-Garcia, M.; Crino, L. MYC and human telomerase gene (TERC) copy number gain in early-stage non-small cell lung cancer. *Am. J. Clin. Oncol-Canc.* **2015**, *38*, 152–158.

(46) Satyanarayana, A.; Manns, M. P.; Rudolph, K. L. Telomeres, telomerase and cancer - an endless search to target the ends. *Cell Cycle* **2004**, *3*, 1138–1150.

(47) Joglekar, M. V.; Satoor, S. N.; Wong, W. K. M.; Cheng, F.; Ma, R. C. W.; Hardikar, A. A. An optimised step-by-step protocol for measuring relative telomere length. *Methods Protoc.* **2020**, *3*, 27.

(48) Zhou, G.; Liu, X.; Li, Y.; Xu, S.; Ma, C.; Wu, X.; Cheng, Y.; Yu, Z.; Zhao, G.; Chen, Y. Telomere targeting with a novel G-quadruplex-interactive ligand BRACO-19 induces T-loop disassembly and telomerase displacement in human glioblastoma cells. *Oncotarget* **2016**, *7*, 14925–14939.

(49) Che, T.; Chen, S.-B.; Tu, J.-L.; Wang, B.; Wang, Y.-Q.; Zhang, Y.; Wang, J.; Wang, Z.-Q.; Zhang, Z.-P.; Ou, T.-M.; Zhao, Y.; Tan, J.-H.; Huang, Z.-S. Discovery of novel schizocommunin derivatives as telomeric G-quadruplex ligands that trigger telomere dysfunction and the deoxyribonucleic acid (DNA) damage response. *J. Med. Chem.* **2018**, *61*, 3436–3453.

(50) Li, Y.; Sun, N.; Ser, H.-L.; Long, W.; Li, Y.; Chen, C.; Zheng, B.; Huang, X.; Liu, Z.; Lu, Y.-J. Antibacterial activity evaluation and mode of action study of novel thiazole-quinolinium derivatives. *Rsc Advances* **2020**, *10*, 15000–15014.

(51) Wurth, C.; Grabolle, M.; Pauli, J.; Spieles, M.; Resch-Genger, U. Relative and absolute determination of fluorescence quantum yields of transparent samples. *Nat. Protoc.* **2013**, *8*, 1535–1550.

(52) Brouwer, A. M. Standards for photoluminescence quantum yield measurements in solution (IUPAC Technical Report). *Pure Appl. Chem.* **2011**, *83*, 2213–2228.

(53) Morris, G. M.; Huey, R.; Lindstrom, W.; Sanner, M. F.; Belew, R. K.; Goodsell, D. S.; Olson, A. J. Autodock4 and autodocktools4: automated docking with selective receptor flexibility. *J. Comput. Chem.* **2009**, *30*, 2785–2791.

(54) Lemarteleur, T.; Gomez, D.; Paterski, R.; Mandine, E.; Mailliet, P.; Riou, J. F. Stabilization of the c-MYC gene promoter quadruplex by specific ligands' inhibitors of telomerase. *Biochem. Biophys. Res. Commun.* **2004**, *323*, 802–808.

Table of Contents Graphic

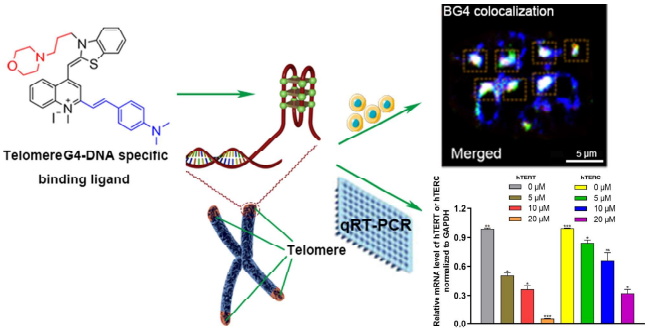

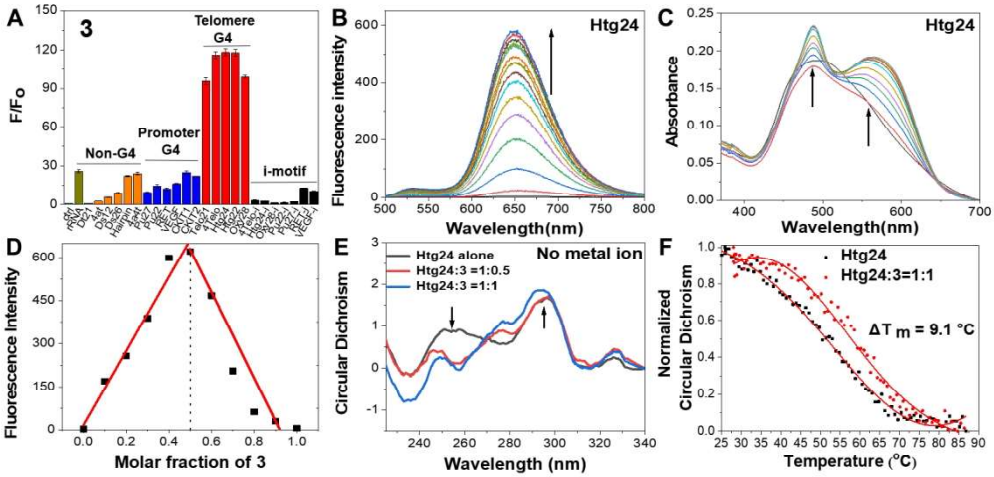
A
3
Telomere G4
Promoter G4
Non-G4
i-motif
F/Fo
B
Htg24
Fluorescence intensity
Wavelength(nm)
C
Htg24
Absorbance
Wavelength(nm)
D
Fluorescence Intensity
Molar fraction of 3
E
Htg24 alone
Htg24:3 =1:0.5
Htg24:3 =1:1
No metal ion
Circular Dichroism
Wavelength (nm)
F
Htg24
Htg24:3=1:1
ΔT m = 9.1 °C
Normalized Circular Dichroism
Temperature (°C)

Figure 1

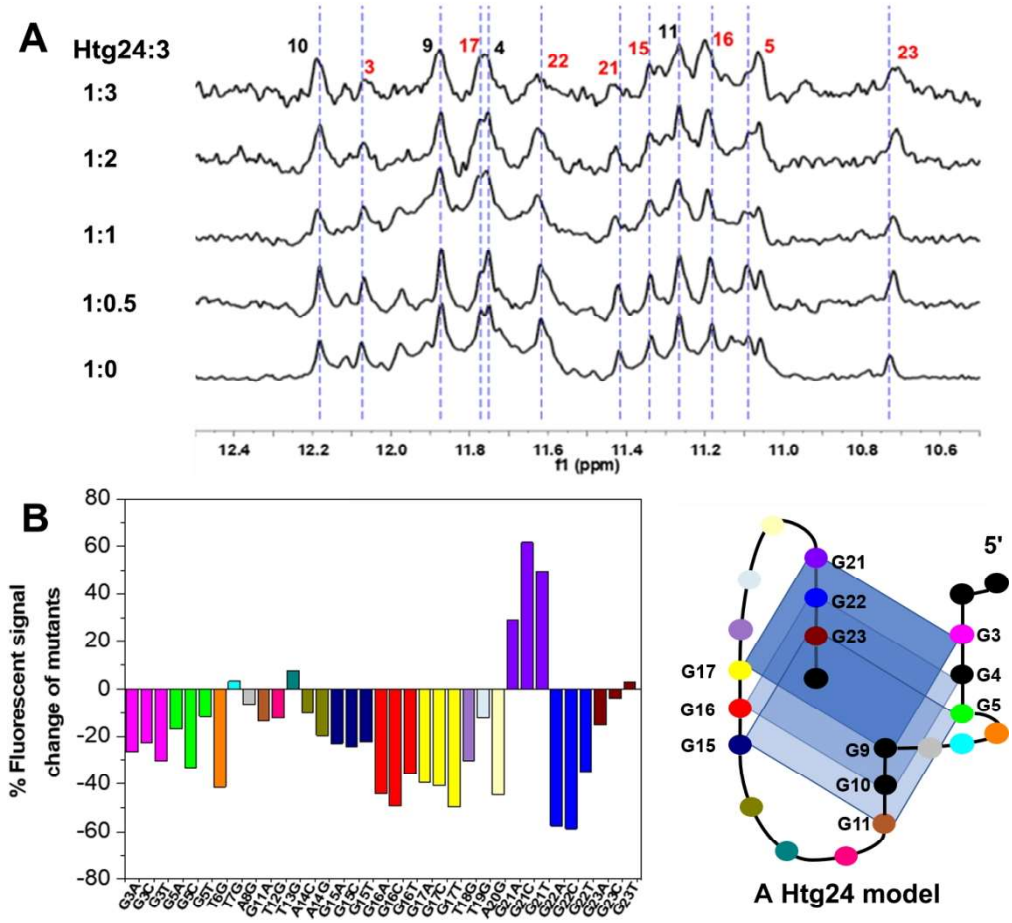
A
Htg24:3
1:3
1:2
1:1
1:0.5
1:0
10
3
9
17
4
22
21
15
11
16
5
23
12.4
12.2
12.0
11.8
11.6
11.4
11.2
11.0
10.8
10.6
f1 (ppm)
B
% Fluorescent signal change of mutants
80
60
40
20
0
-20
-40
-60
-80
G21
G22
G23
G3
G4
G5
G9
G10
G11
G15
G16
G17
5'
A Htg24 model

Figure 2

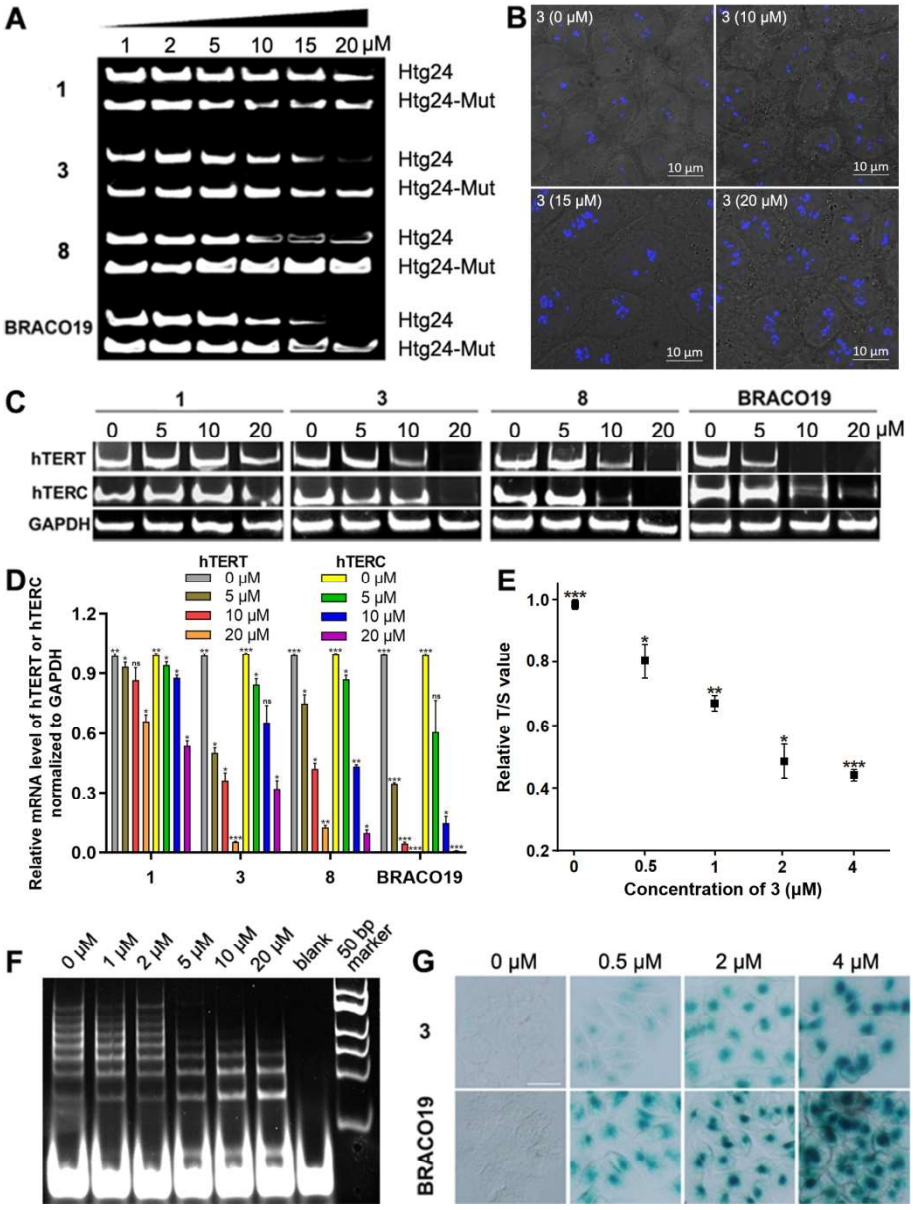
A
1 2 5 10 15 20 μM
1
3
8
BRACO19
Htg24
Htg24-Mut
B
3 (0 μM)
3 (10 μM)
3 (15 μM)
3 (20 μM)
10 μm
C
1 3 8 BRACO19
0 5 10 20 μM
hTERT
hTERC
GAPDH
D
hTERT
hTERC
0 μM
5 μM
10 μM
20 μM
Relative mRNA level of hTERT or hTERC normalized to GAPDH
1 3 8 BRACO19
E
Relative T/S value
Concentration of 3 (μM)
F
0 μM 1 μM 2 μM 5 μM 10 μM 20 μM blank 50 bp marker
G
0 μM 0.5 μM 2 μM 4 μM
3
BRACO19

Figure 3

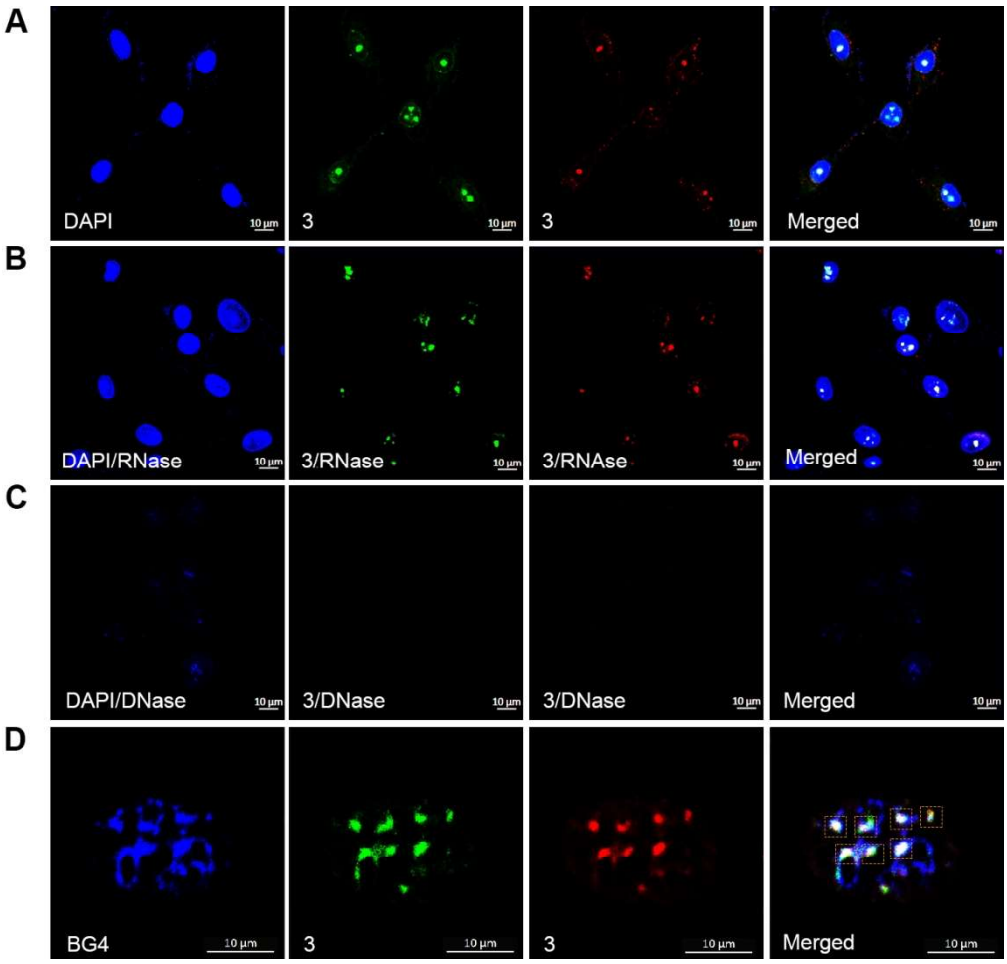
A
DAPI
10 μm
3
10 μm
3
10 μm
Merged
10 μm
B
DAPI/RNase
10 μm
3/RNase
10 μm
3/RNAse
10 μm
Merged
10 μm
C
DAPI/DNase
10 μm
3/DNase
10 μm
3/DNase
10 μm
Merged
10 μm
D
BG4
10 μm
3
10 μm
3
10 μm
Merged
10 μm

Figure 4

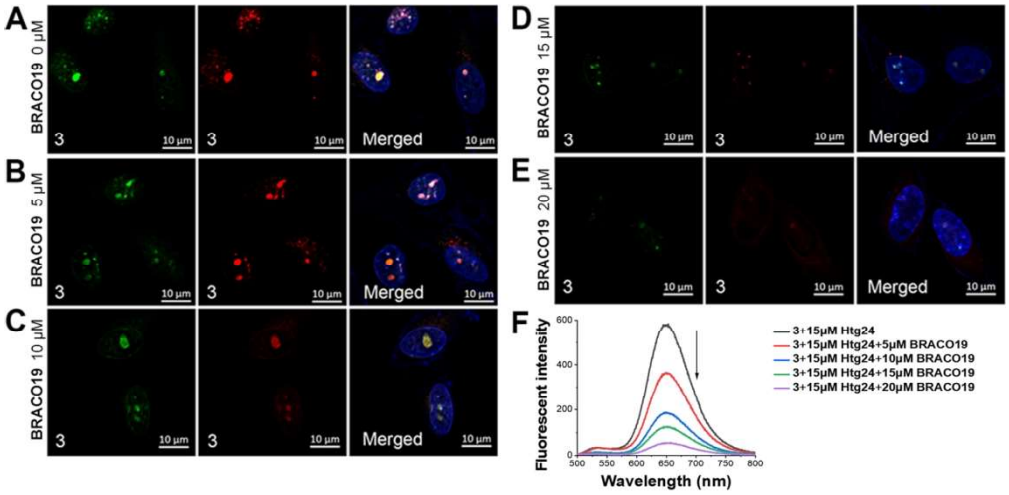
A
BRACO19 0 μM
B
BRACO19 5 μM
C
BRACO19 10 μM
D
BRACO19 15 μM
E
BRACO19 20 μM
3
Merged
10 μm
F
Fluorescent intensity
Wavelength (nm)
3+15μM Htg24
3+15μM Htg24+5μM BRACO19
3+15μM Htg24+10μM BRACO19
3+15μM Htg24+15μM BRACO19
3+15μM Htg24+20μM BRACO19

Figure 5

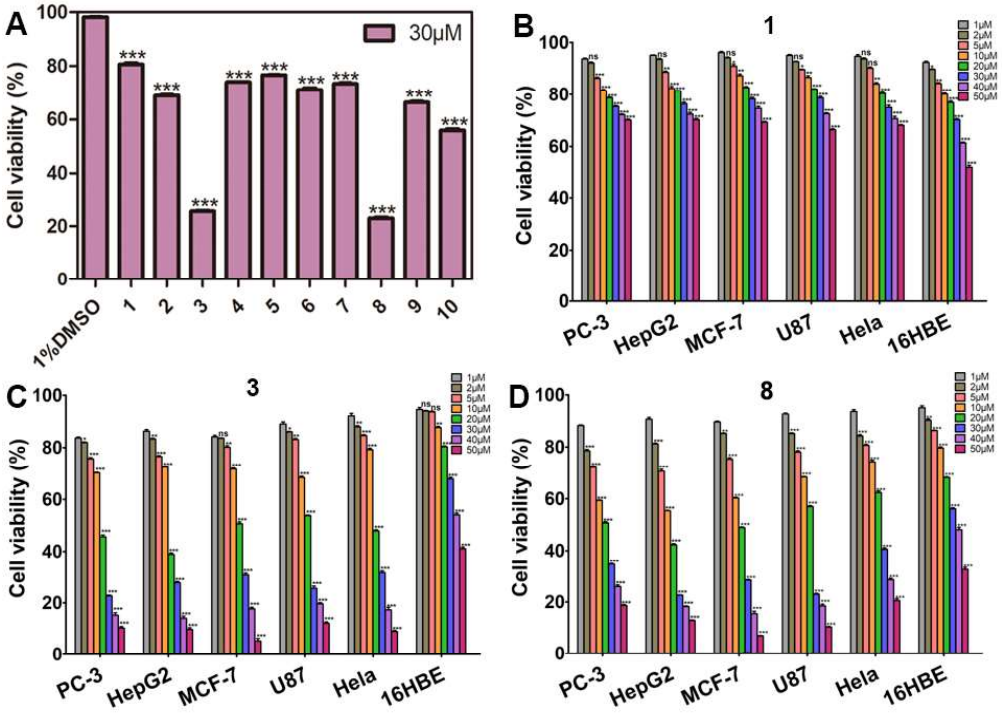
A
30μM
Cell viability (%)
1%DMSO
1
2
3
4
5
6
7
8
9
10
B
1
C
3
D
8
PC-3
HepG2
MCF-7
U87
Hela
16HBE

Figure 6

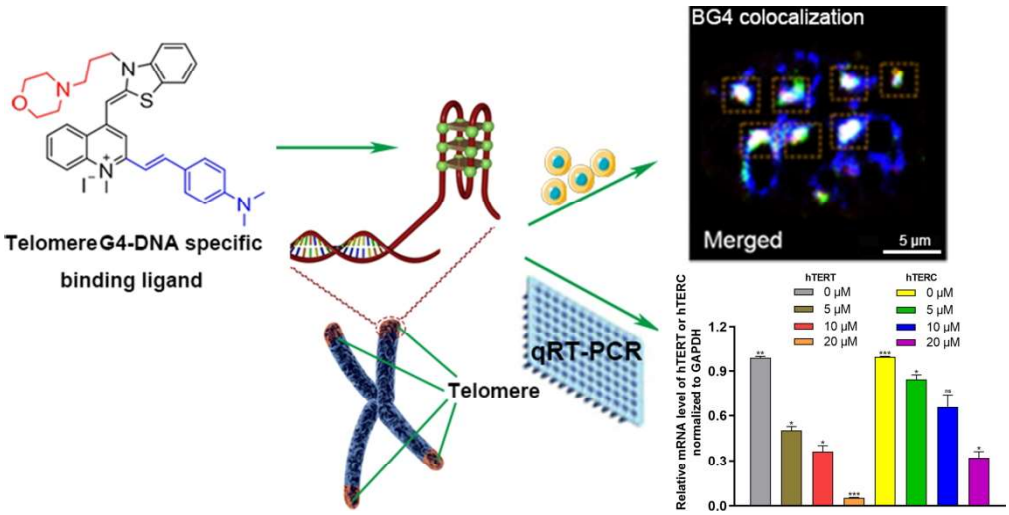

Table of Contents Graphic